American Journal of Nano Research and Applications
2018; 6(2): 34-53
http://www.sciencepublishinggroup.com/j/nano
doi: 10.11648/j.nano.20180602.11
ISSN: 2575-3754 (Print); ISSN: 2575-3738 (Online)

Review Article

Review of GaN/ZnO Hybrid Structures Based Materials and Devices

Ahmed Mohammed Nahhas

Department of Electrical Engineering, Faculty of Engineering and Islamic Architecture, Umm Al Qura University, Makkah, Saudi Arabia

Email address:
amnahhas@uqu.edu.sa

To cite this article:
Ahmed Mohammed Nahhas. Review of GaN/ZnO Hybrid Structures Based Materials and Devices. *American Journal of Nano Research and Applications*. Vol. 6, No. 2, 2018, pp. 34-53. doi: 10.11648/j.nano.20180602.11

Received: May 10, 2018; **Accepted**: May 28, 2018; **Published**: June 15, 2018

Abstract: This paper presents a review of recent advances of Gallium Nitride (GaN) and Zinc Oxide (ZnO) based hybrid structures materials and devices. GaN and ZnO have gained substantial interest in the research area of wide bandgap semiconductors due to their unique electrical, optical and structural properties. GaN and ZnO are important semiconductor materials with applications in blue and ultraviolet (UV) optoelectronics. Both materials have similar physical properties. GaN and ZnO as hybrid material have received much attention due to their unique potential applications. Several potential optical applications are being fabricated based on GaN and ZnO hybrid materials such as optical wave guide, light emitting diodes (LEDs), and laser diodes (LDs). The recent aspects of GaN and ZnO hybrid *based* devices are presented and discussed.

Keywords: GaN, ZnO, Nanostructured, Hybrid, Light Emitting Diodes, Nanowires, Multiple Quantum Wells (MQW), UV

1. Introduction

ZnO is a group II-VI compound semiconductor material, with a direct wide bandgap of 3.37 eV and a large exciton binding energy of 60 meV [1]. This binding energy is significantly high, 2.4 times the room temperature thermal energy which permits the fabrication of ZnO based photoelectronic devices possessing high optical efficiency, while the wide bandgap eases the application of ZnO thin films for short wavelength optoelectronic devices [2]. The unique physical properties of ZnO has numerous advantages for the electronic device due to the improved carrier confinement in one-dimension, increased junction area and hole transport. The conjugated polymer has higher hole mobility while the ZnO has higher electron mobility. When ZnO mixed with other materials, it makes good electronic properties [3]. ZnO has impressive electronic and optical properties. Due to these properties, ZnO has received a considerable attention in a wide range of applications such as transparent conductive oxide, optoelectronic, and piezoelectric devices [4-6]. Recently, ZnO has attracted increasing interest in organic and amorphous semiconductor for plastic electronic, LEDs, photodetector (PD), solar cells (SCs), and transparent thin film transistors [7].

ZnO normally has a hexagonal structure with a = 3.25Å and c = 5.12 Å; each Zn atom is tetrahedrally coordinated to four oxygen atoms, where the zinc d-electrons hybridize with the oxygen p-electrons; layers occupied by Zn atoms alternate with layers occupied by oxygen atoms [8]. Moreover, the crystalline structure of the ZnO exists as wurtzite and Zn blende, which led it as a perfect polar symmetry along the hexagonal axis, which is responsible for a number of the physical and chemical properties, including piezoelectricity and spontaneous polarization.

ZnO has been widely investigated for its potential in optoelectronic devices such as varistors, UV sensors, biosensors [9], optical wave guides, UV light emitters [10], LEDs [11], piezoelectric micro electro mechanical systems (MEMS) [12], chemical sensors [13], pH sensors, spin electronics [14], solar energy [15], p-n junctions [16], field effect [17], field sensors [18], gas sensors [19], temperature sensors [20], field emission [21], display [22], catalysis [23], acoustic wave [24], and SCs [25].

ZnO is categorized as n-type semiconductor. It is between covalent and ionic bond of semiconductor [26]. Recently, the composite of ZnO n-type semiconductor and conjugate

polymer *p*-type are very introducing for organic LEDs. The conjugated polymers poly [2-methoxy-5-2′-ethyl-hexyloxy-1,4-phenylenevinylene] (MEH-PPV) [27] containing inorganic material have been subject of a considerable research because of their potential electrical, structural and optical characteristics for optoelectronic device. The conjugated polymer is used in optoelectronic especially in emitting device due to its good electrical conductivity and high stability [28]. ZnO thin films have been fabricated using variety of techniques including sol-gel technique, radio frequency (RF) magnetron sputtering, pulsed laser deposition (PLD), electron beam evaporation (e-beam), spray pyrolysis, metal organic chemical vapor deposition (MOCVD), and molecular beam epitaxy (MBE), electrochemical deposition method [29]. The electrochemical deposition method, which is one of the wet processes, is a well-established solution based process to obtain ZnO thin films [30] and has some advantages such as low cost and low temperature deposition over vapor phase deposition [31].

2. GaN Properties

GaN has a direct wide bandgap of 3.4 eV. GaN has superior electronic properties, such as low electron affinity (2.7-3.3 eV), high melting point (2600 K), and small work function (4.1 eV) [32], which are of great performance for field emission (FE) devices such as cold cathode emitters and flat panel display [33]. GaN based devices are highly suitable for high frequency, high power, and high temperature electronics applications [34]. GaN based materials demonstrate several high level electronic and material properties such as a high breakdown electrical field, high saturation velocity, high thermal stability [35] and chemical inertness [36]. Due to these properties, GaN is considered as a well-established semiconductor used in solid state lighting devices [37] and in high temperature as well as high power operation electronic applications [38-40]. GaN material is a chemically and mechanically stable. It has a high thermal conductivity and a high mobility [41, 42]. GaN material is considered as an excellent choice for efficient and durable device fabrication [43-45].

GaN based devices have promising prospects in military, satellite and commercial applications. Several devices can be fabricated based on GaN including light detecting and emitting devices, such as solar blind detectors, LEDs [46], and blue/green/UV LDs [46]. Moreover, GaN has gained much attention due to its potential applications in series of devices such as LEDs, short wavelength emitters or detectors, high power and high frequency electronic devices [47-49]. GaN based LEDs are widely applied in color displays, traffic lights, and solid state lighting [50-52]. GaN based semiconductors are highly promising for the fabrication of electronic devices including high electron mobility transistors [53], heterojunction bipolar transistors [54], UV Schottky barrier photodetectors (PDs) [55], and metal semiconductor metal (MSM) PD [56]. To enhance the efficiency of these electronic devices, the formation of high quality ohmic and Schottky contacts is crucial [57, 58]. On the other hand, GaN is an essential material for high frequency and high power devices with applications in wireless communication and electric transportation systems [59, 60]. GaN based heterostructure devices remain a big concern for the commercial success [61]. The polarization effects including piezoelectric and spontaneous polarization in one way are found to be useful in heterostructure devices, whereas the same properties are seen to be a curse due to the responsible for threshold voltage shift heterostructures and delivering lower output power in the nitride based LEDs [62, 63]. Doped and undoped GaN has been widely used in several optoelectronic devices due to its ability to cover a wide spectral range, as well as due to its high electrical conductivity comparing to other III-V semiconductors [64-66]. GaN can be doped with different types of impurity elements including silicon [67], magnesium [68], copper [69], cobalt [70], mercury [71], aluminum [72], germanium [73], and titanium [74]. The electronic properties of GaN could be controlled through modifying the type as well as the content of dopants [75].

3. GaN and ZnO Properties

GaN and ZnO have wurtzite crystal structures with identical in plane lattice parameter. The bandgap energies of ZnO and GaN are similar. ZnO have a larger exciton binding energy comparing with GaN, 60 meV and 26 meV respectively [76]. They both crystallize in the hexagonal wurtzite structure and have a direct bandgap of about 3.4 eV at low temperatures [77]. GaN and ZnO are the most important wide bandgap semiconductor materials currently being used for the short wavelength optoelectronics industry. The two materials have similar properties in many aspects [78]. GaN and ZnO are suitable for applications in optoelectronics high temperature, high frequency and high power devices [79]. GaN and ZnO are the most wide bandgap semiconductor materials that have been recently attracting much interest due to their promise for application in electronic and optoelectronic devices [80].

GaN and ZnO are the most important semiconductor materials for the application of optoelectronic devices such as blue LED, blue LD, and UV PD [81-83]. GaN and ZnO have been used to fabricate blue, green, and UV LEDs, LDs, UV blind detectors, high power, and high temperature electronics. They also have superior electrical properties, including controllable conductivity and a higher carrier mobility than organic materials [84, 85]. However, the practical device application using ZnO is still undergoing inherent problems including lacks of reproducibility on forming the stable *p*-type ZnO layer and availability on engineering the bandgap energy [83]. GaN and ZnO are among the inorganic semiconductor materials [85]. Among the inorganic semiconductor materials, ZnO has been investigated and demonstrated its capability of constructing high quality optoelectronic and inorganic devices [86-88].

4. Hybrid Organic and Inorganic Materials Properties

Organic and inorganic semiconductor hybrid structures have received much attention due to their unique properties. The combined structures can be used in novel devices and many practical applications [89-91]. The unique properties resulted from the combination of the two materials allow such structures to be used in novel optoelectronic devices and many applications [85, 89-91]. Recently, the organic/inorganic semiconductor hybrid structures have attracted a considerable attention due to their strong potential for applications such as efficient microlight sources that can be used in full color displays, imaging systems, miniature chemical and biological sensors [92]. The coupling of organic and inorganic semiconductors allows to utilize the most favorable properties of the inorganic component, e.g. the high electrical conductivity, with the most favorable properties of the organic component, e.g. the high photoluminescence (PL) yield across the visible spectrum [93]. The organic and the inorganic hybrid system has been developed to provide a potential platform for the optoelectronic applications, such as tunable photodiodes [94], transparent coatings for short wavelength shielding [95], light up conversion devices [96], hybrid SCs [97-99]. On the other hand, the organic semiconductors have excellent luminescence properties with a greater variety of emission wavelengths, significantly higher PL efficiencies and potential for stable *p*-type electrodes; however, they exhibit inferior electrical behaviors [85, 100, 101]. The organic semiconductors have many advantages, such as high absorption coefficient, variable bandwidth, low cost and excellent manufacturing performance [88, 102, 103]. They have attracted keen attention due to their potential for the next generation optoelectronic devices including displays, lightings, and logic circuits [104, 105]. The organic light emitting devices (OLEDs) have been successfully launched in market as a display in smart phones and high density televisions [106]. In addition, for the last decade, organic solar cells (OSCs) have been intensively studied because of their expectations for low cost production of light and flexible plastic solar modules [107]. Recently, the power conversion efficiency of OSCs reached 11% by employing new semiconducting polymers and developing new device structures [108, 109, 110]. The organic photodetectors (OPDs) have been less spotlighted than OLEDs and OSCs, even though they possess the same advantages as for OSCs and huge applications as cameras or sensors for smart phones, notebooks, industrial monitoring systems, cars, aircrafts, and military systems [111, 112]. There are many benefits of the OPDs such as large area, ultrathin, light weight and flexible and bendable detectors, compared to conventional inorganic PDs [113, 114]. The organic *and* inorganic hybrid SCs with perovskite structure have been widely studied because of the easy of fabrication process and the high power conversion efficiency [115-118]. The power conversion efficiencies of these devices strongly depend on the device structures and the fabrication processes [119].

5. ZnO Based Devices

ZnO devices based on hybrid organic and inorganic materials have attracted a considerable attention, both in basic research and applications because they offer the possibility of combining the stability and the tunable electronic properties of inorganic semiconductors with the large functionality and the selectivity of organic chemistry [120]. The ZnO organic OLEDs are promising for lightings and flexible displays because OLEDs have high contrast, surface emission, and light weight in contrast to inorganic LEDs. In the device structure of conventional OLEDs, it is essential to deposit low work function and air sensitive cathode materials, such as calcium and barium, and to encapsulate rigorously because of the protection from moisture and oxygen. Recently, ZnO inverted OLEDs (IOLEDs) have received a considerable attention because they are air stable and thus, suitable for flexible OLED displays [121]. The IOLEDs configuration is inverted with respect to that of conventional OLEDs. The device structure of the IOLEDs is substrate/metal oxide cathode/light emitting polymer/MoO_3/Au anode. The main advantage of IOLEDs is that metal oxides work as electron injecting layers (EILs), avoiding the use of reactive cathodes and therefore allowing the devices preparation without rigorous encapsulation. The air stable metal oxide EILs in IOLEDs are based on several materials such as titanium oxide (TiO_2) [122] and ZnO [123]. The recent important approach has been using the ZnO thin films as EILs in IOLEDs because the IOLEDs with the ZnO EIL exhibits relatively high current efficiency [124, 125] resulting from the favorable conduction band energy level, high transparency and high electron mobility of ZnO thin films [125].

The study of the ZnO photonic crystal (PC) formed via facile nanoimprinting employed on the ZnO electron selective layer of inverted organic photovoltaics (OPV) was reported by Nirmal et al. [126]. The optimized inverted OPV fabricated with these highly ordered periodic structures provided effective light trapping, which resulted in increased incident light absorption in the active layer [126]. Consequently, the OPVs with the ZnO PC layers showed a 23% current density improvement compared with OPVs with planar ZnO layer [126]. The time domain simulation of the finite difference study showed that the electric field intensity was significantly higher in the active layer for devices with ZnO PC structures in comparison with reference devices with planar ZnO electron selective layer [126]. The nano imprinted ZnO PC is, thus, a viable method for the light absorption and the efficiency enhancement in OPVs [126]. The study's result showed that the PCs embedded in the electron selective layer of the OPV lead to the enhancement of the current density by virtue of field localization. The optimized OPVs with these PC structures can effectively trap the incident light and increase the absorption in the active layer [126]. The ZnO PC provided an enhanced performance [126]. The use of such photonic structures could be readily extended to any metal oxide interlayer employed in OPV structures. The low refractive index of the ZnO PC structure with P3HT:PCBM active layer

provided the index contrast necessary for the field localization provided by the photonic crystal and, thus, aids in increasing the optical path length of incident light [126]. It enhances subsequently the optical absorption in the active layer [126]. Figure 1 shows the schematic representation of the fabricated OPV devices. Figure 2 shows the scan electron microscopy (SEM) image of the ZnO PC structure formed on ITO coated glass [126]. Figure 3 shows the I-V characteristics of the OPV devices with the planar ZnO and the ZnO photonic crystal electron selective layers [126].

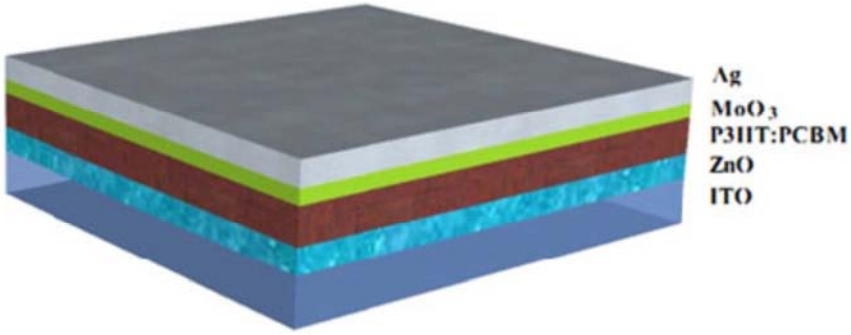

Figure 1. *Schematic representation of the fabricated OPV devices [126].*

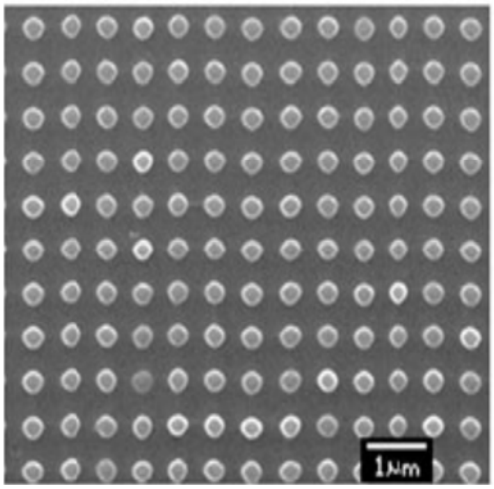

Figure 2. *SEM image of the ZnO PC structure formed on ITO coated glass [126].*

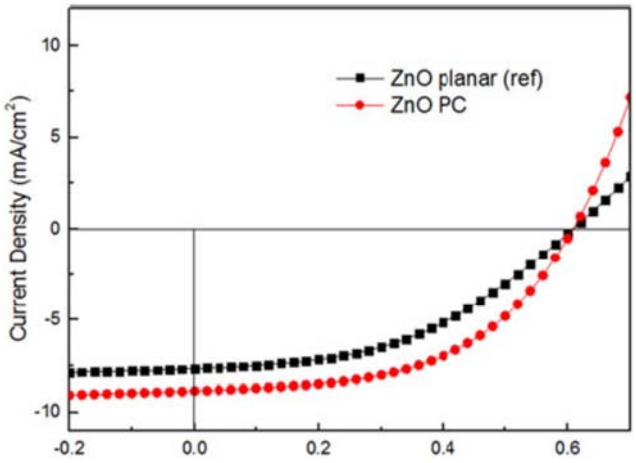

Figure 3. *I-V characteristics of OPV devices with the planar ZnO and the ZnO PC electron selective layers [126].*

The high efficiency OPV with a PTB7: PC_{70} BM photo absorption layer was fabricated by adopting *Lithium* (Li)- and *Cadmium* (Cd)-doped ZnO electron extraction layers was reported by Kim et al. [127]. For devices with both Li- and Cd-doped ZnO, the performance was significantly improved, including the short circuit current, the open circuit voltage, the fill factor (FF), and the power conversion efficiency [127]. The resulted films were characterized by the X-ray diffraction (XRD), the high resolution the transmission electron microscopy (TEM), and the resistivity analysis. The study's results suggested that the improved electrical properties of Li- and Cd-doped ZnO electron extraction layers with a doping ratio of approximately at 6% are highly effective in achieving a power conversion efficiency of up to 8% [127]. The Cd-doped ZnO showed better electrical properties attributed to Cd in the substitutional sites along with increased carrier density compared with that of pristine ZnO [127]. The power conversion efficiency (PCE) was significantly improved to 7.90% [127]. These results are contributed to the use of the interfacial engineering with Li and Cd dopants into the ZnO electron extraction layer in OPVs to facilitate the efficiency improvement [127]. Figure 4 shows the OPV device architecture [127]. Figure 5 shows the TEM of ZnO [127].

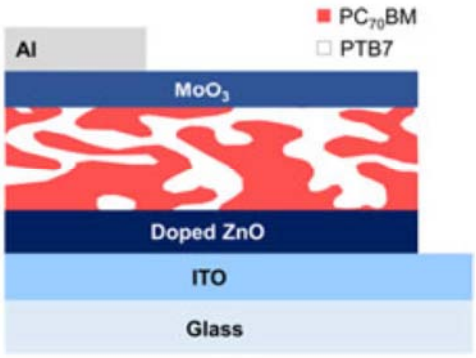

Figure 4. *OPV device architecture [127].*

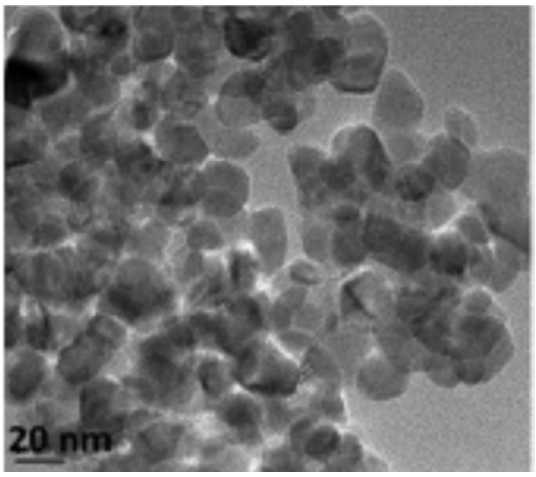

Figure 5. *TEM of ZnO [127].*

The fabrication of the inverted type OPDs with ZnO electron collecting buffer layers and polymer was reported by Jeong et. al [128]. The visible light was detected by the inverted OPDs when a background UV light was ON, whereas no photocurrent signal was measured for visible lights without the background UV light [128]. The UV lights solely were successfully detected without any surrounding UV light [128]. The devices exhibited fast and stable photoresponse under the modulated or the continuous UV visible lights [128]. The study's results showed that the external quantum efficiency (EQE) value was significantly enhanced by increasing the applied voltage, and the corrected responsivity (RC) reached 2000 mA/W at a lower light intensity [128]. The devices could sense the UV lights without the background UV illumination [128]. The light modulation and stability test proved that the present OPDs were quite stable enough for practical UV-visible detector applications by further optimization [128]. Figure 6 shows the device structure and the materials used for the inverted OPD [128]. Figure 7 shows the I-V characteristics of the devices under the illumination of a monochromatic light 525 nm, 113 μW/cm^2 with UV ON or without UV OFF the background UV illumination 365 nm, 177 μW/cm^2 [128].

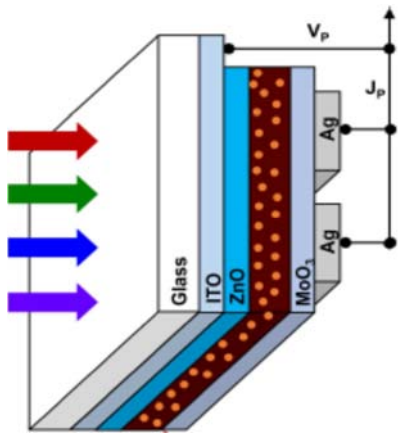

Figure 6. *Structure and materials used for the inverted fabricated Device [128].*

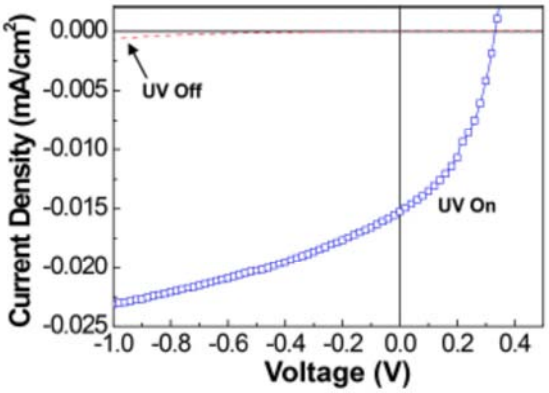

Figure 7. *I-V characteristics of the devices under illumination of a monochromatic light 525 nm, 113 μW/cm^2 with UV ON or without UV OFF the background UV illumination 365 nm, 177 μW/cm^2 [128].*

The performance of the conventional bulk heterojunction (BHJ) OSC incorporating a solution processed ZnO spin coated on the photoactive layer poly 3-hexylthiophene: indene-C_{60} b_{is} adduct was reported by Kim et al. [129]. The study showed a significant improvement in short circuit current density (J_{sc}) upon the introduction of ZnO. That improvement is further evidenced by the reduction of J_{sc} leading to a lower power conversion efficiency (PCE) in the device without the presence of ZnO [129]. The effect of the photomask on the ZnO based device's performance cause a decrease in both the J_{sc} and the open circuit voltage (V_{oc}) [129]. The decrease is about 13.42% and 0.73%, respectively. But it causes an increase in the filling factor (FF) [129]. Although the introduction of the photomask on the device active area decreased both J_{sc} and V_{oc}, it actually increased the FF to 55%; thus, the PCE in the case with the photomask effect has been reduced to 4.42% [129] Hence, serious carefulness must be taken to define the accurate active area and the photomask area [129]. The studied device showed a good lifetime in which the PCE only drops by 18.04% although the measurements were conducted up to 1440 h [129]. The study's results demonstrated that the ZnO plays an important role in the improvement of the OSCs' performance [129]. Figure 8 shows the layer sequence of the conventional BHJ OSCs. Figure 9 (a) shows the current density of the devices with and without ZnO, (b) the current density before and after the photomask. A V_{oc} of up to 0.818 V was obtained in the device based on the ZnO [129].

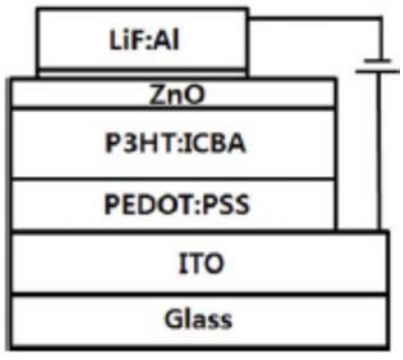

Figure 8. *Layer sequence of the conventional BHJ OSCs [129].*

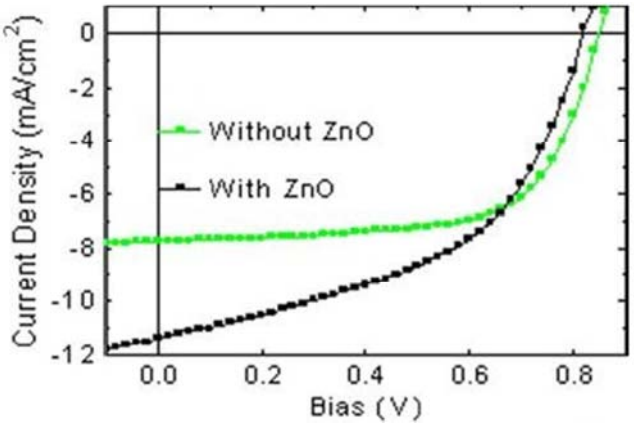

(a)

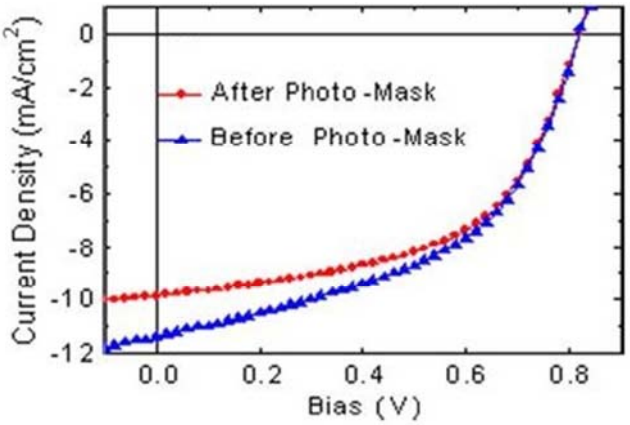

(b)

Figure 9. *(a) I-V characteristics of the devices based with/without ZnO (b) I-V characteristics of a device based on ZnO before and after photomask [129].*

The electrical and the optical properties of the poly dioctylfluorene-alt-benzothiadiazole based IOLEDs with electrochemically deposited ZnO EIL have been reported by Takada et al. [130]. The device characteristics of the fabricated IOLEDs were comparable to those of conventional IOLEDs with sputtered ZnO EIL, indicating that the electron injection properties of the electrodeposited ZnO EIL were similar to those of the sputtered ZnO EIL [130]. The impedance spectroscopy revealed that the equivalent circuits of IOLEDs with electrochemically deposited ZnO EIL and with sputtered ZnO EIL are indistinguishable [130]. The study's results showed that the equivalent circuits below and above the electroluminescence (EL) threshold in IOLEDs with electrodeposited ZnO EIL were the same as those in the IOLEDs with the sputtered ZnO EIL [130]. Figure 10 shows the schematic structure of the IOLEDs. Figure 11 shows the SEM images of the ZnO deposited by an electrochemical method on ITO substrate [130]. Figure 12 (a) shows the plots of the current density versus applied voltage for IOLEDs [130], (b) the luminance versus the applied voltage for IOLEDs [130].

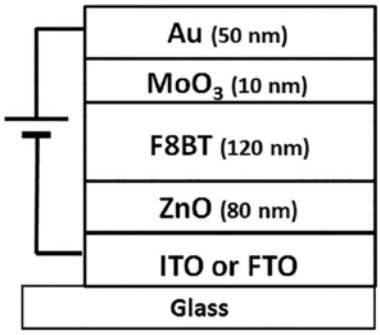

Figure 10. *Schematic structure of IOLEDs [130].*

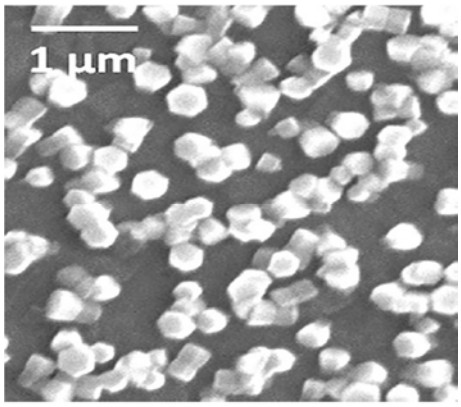

Figure 11. *SEM images of ZnO deposited on ITO substrate [130].*

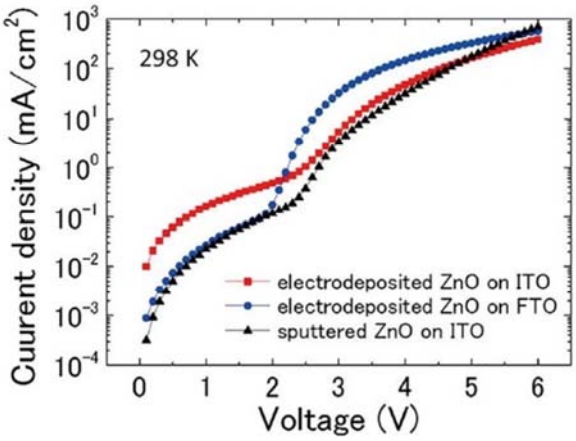

(a)

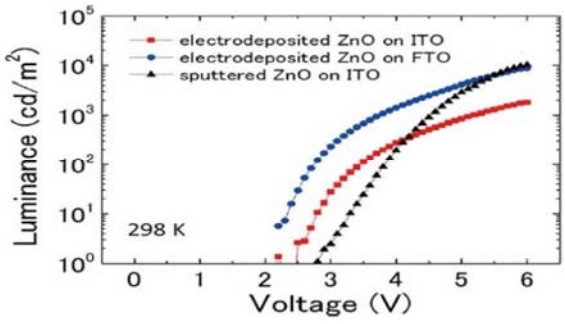

(b)

Figure 12. *(a) current density versus applied voltage (b) luminance versus applied voltage for IOLEDs [130].*

The fabrication of the inorganic flexible LEDs using CuO and ZnO nanowires as the hole and electron transport materials was reported by Biswas et al. [131]. The flexible inorganic *p*-CuO nanowires/*n*-ZnO nanowires heterojunction LED was fabricated on polyimide (PI) substrates [131]. Both the metal oxide semiconductors were synthesized by the using of low temperature 100 ^{o}C solution processes [131]. The synthesized CuO nanowires were chemically pure and exhibited agglomerating and flexible nature [131]. The heterojunctions were fabricated inside 5 mm square patterns in order to achieve better flexibility [131]. The study's results showed that the I-V characteristics of the heterojunction revealed a typical p-n diode nature with an on/off ratio of 8.6 x 10^2 at 4 V, a turn on voltage of 2.8 V, and a stable current flow at different voltage stress [131]. The EL spectra from the LED at different forward bias exhibited eminent peak at around 710 nm corresponding to red light, which was in accordance with the deep level emission of PL spectra of the ZnO nanowires [131]. The X-ray photoelectron spectra revealed that the deep levels are related to the oxygen vacancies (V_Os) [130]. The devices showed a significant stability during the bending test and continued to emit light beyond 1000 cycles of the dynamic bending at a curvature radius of 5 mm [131]. The EL spectra and the corresponding optical microscopic (OM) images of the heterojunction LED revealed a stable red emission with an eminent peak at 710 nm. The emission was originated from the radiative recombination through V_Os in the ZnO nanowires which was in accordance with the deep level emission (DLE) of PL spectra [131]. The presence of V_Os was also confirmed by the Zn *2p* and O *1s* narrow scan X-ray photoelectron spectroscopy (XPS) spectra [131]. The light emission was observed to be promising up to 500 cycles of the dynamic bending with a curvature radius of 5 mm [131]. The LEDs continued to emit light beyond 1000 cycles of dynamic bending indicating a robust nature [131]. Figure 13 shows the schematic illustration of the multistep fabrication process of the inorganic flexible LEDs (a) flexible PI substrate of 20 µm thickness (b) the deposition of the 100 nm aluminum for ohmic contact with *n*-ZnO (c) flexible PI substrate after the deposition of Gallium doped ZnO (GZO) seed layer 100 nm (d) 1.5 µm-thick patterned photoresist on flexible PI using the optical lithography [131]. Figure 14 shows the SEM image of ZnO nanowires indicating an average length of 500 nm. The figure inset shows the nanowires at higher resolution showing an average diameter of 50 nm. Figure 15 shows the I-V characteristics of the heterojunction LED revealing a typical p-n diode nature. Figure 16 shows the LED EL spectra under the dc forward voltages. The inset shows the variation of the EL intensity and the full width half maximum (FWHM) of the spectra as a function of the applied voltage [131].

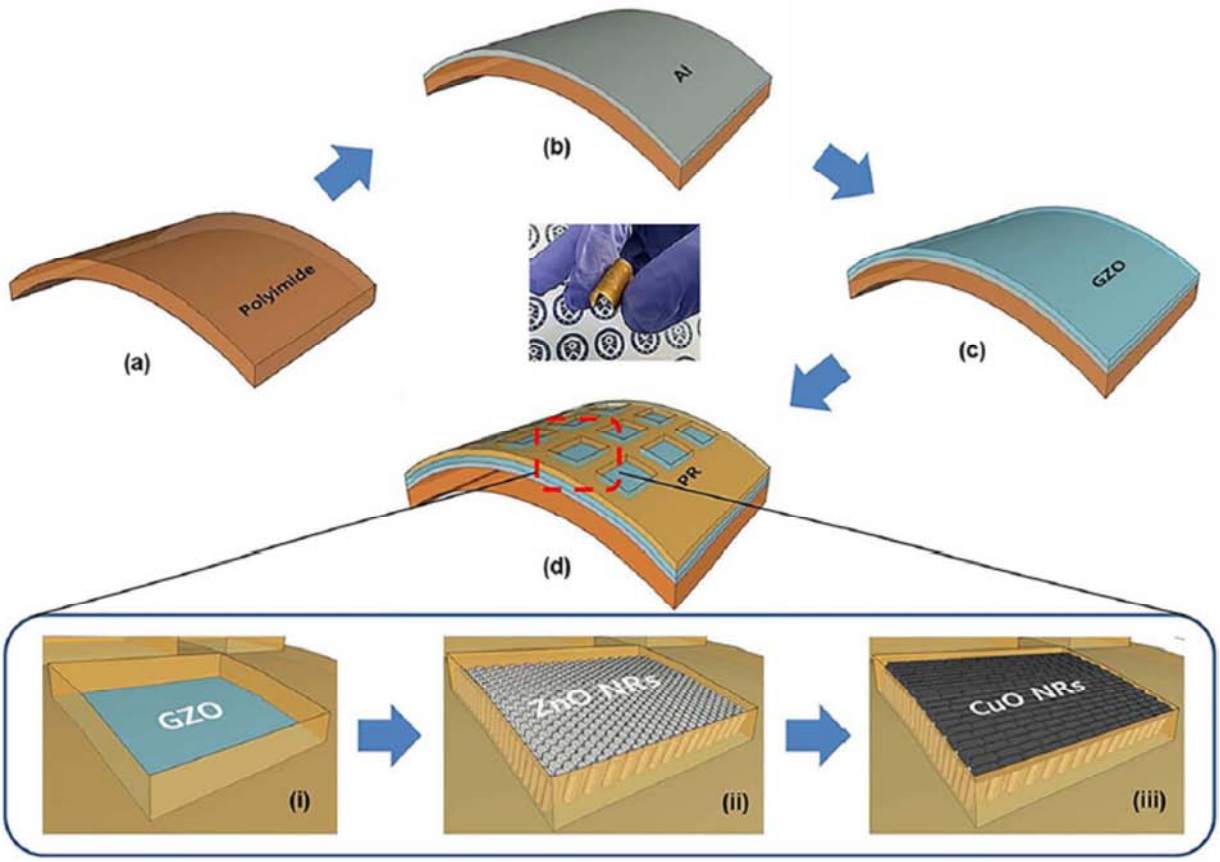

Figure 13. *Schematic of the multistep fabrication process of inorganic flexible LEDs: (a) Flexible PI substrate of the thickness of 20 µm (b) Deposition of aluminum 100 nm for ohmic contact with n-ZnO (c) Flexible PI substrate after deposition of GZO seed layer 100 nm (d) 1.5 µm-thick patterned photoresist on flexible PI using optical lithography [131].*

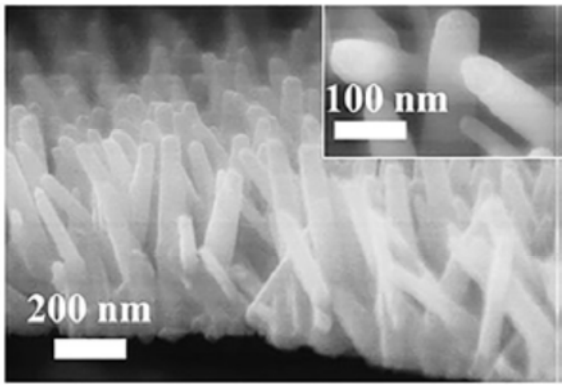

Figure 14. *SEM image of ZnO nanowires with average length of 500 nm: inset shows nanowires at higher resolution with an average diameter of 50 nm [131].*

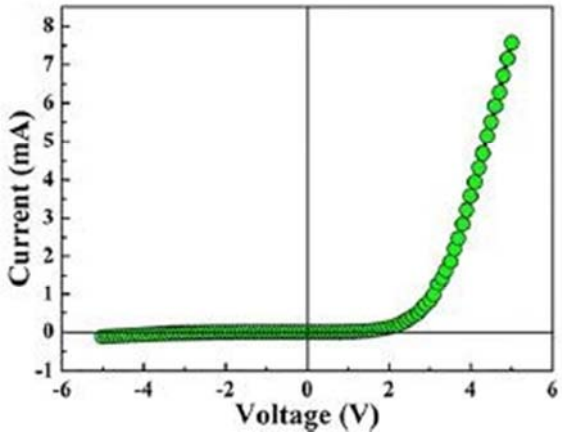

Figure 15. *I-V characteristics of the heterojunction LED revealing a typical p-n diode nature [131].*

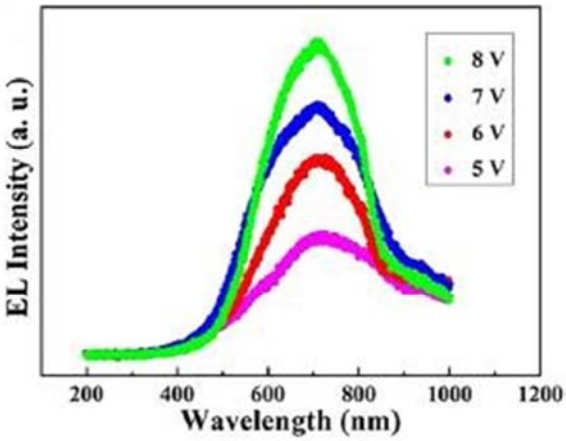

Figure 16*. LED EL spectra under the same dc forward voltages: inset shows the variation of EL intensity and FWHM of the spectra as a function of applied voltage [131].*

The effect of the buffer layers for the OSC, the nanorod like TiO_2 and ZnO thin films onto the Indium Tin Oxide (ITO)/glass using sol-gel and electrochemical method was reported by Thao et al. [132]. The TiO_2 films were crystallized in the anatase phase and the ZnO films, in the wurtzite structure. The nanorods in both films have a similar size of 15 to 20 nm in diameter and 30 to 50 nm in length [132]. The nanorods have an orientation nearly perpendicular to the ITO substrate surface [132]. The TiO_2 bandgap and ZnO films were determined to be 3.26 eV and 3.42 eV, respectively [132]. The laminar OSCs with added TiO_2 and ZnO, namely ITO/TiO_2/P3HT: PCBM/LiF/Al TBD and ITO/ZnO/P3HT: PCBM/LiF/Al ZBD were made for the characterization of the energy conversion performance [132]. The study's result showed that the nanorod like ZnO film was found to be a much better buffer layer that made the FF improve from a value of 0.60 for the TBD to 0.82 for the ZBD, and consequently the PCE was enhanced from 0.84 for TBD to 1.17% for the ZBD [132]. The nature and nanostructures of a buffer layer can thus influence greatly the performance of OSCs [132]. Figure 17 shows the field emission scanning electron microscopy (FESEM) of the ZnO/ITO/glass. Figure 18 shows the XRD patterns of the ZnO/ITO [132].

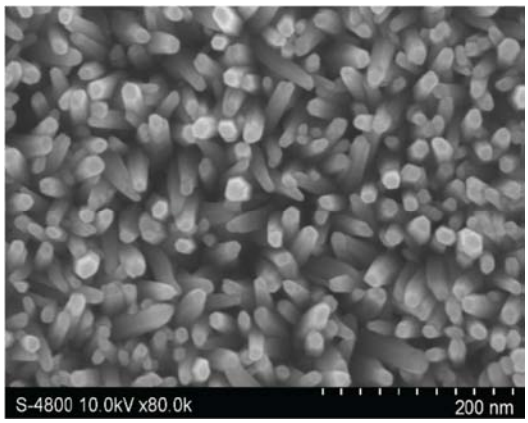

Figure 17. *FESEM of ZnO/ITO/glass thin films [132].*

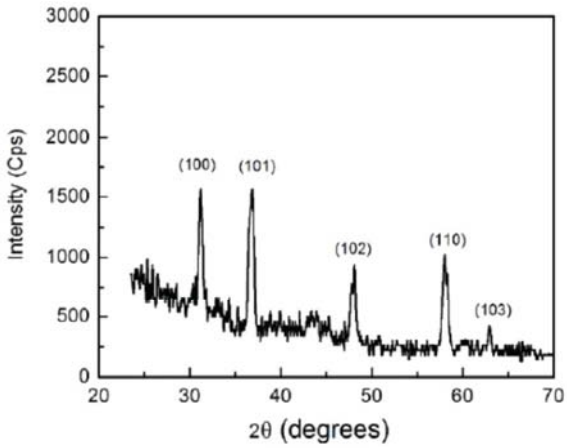

Figure 18. *XRD patterns of the ZnO/ITO [132].*

The organic/inorganic hybrid UV photovoltaic detector using the Polyfluorene (PFO)/ZnO heterojunction was developed and reported by Guo et al. [133]. The device structure aluminum/PFO/ZnO/ITO had a smooth surface *root mean square* (RMS) roughness: 0.28 nm which is a key parameter for the large array, high uniformity UV focal plane array (FPA) detectors [133]. The PFO/ZnO heterojunction may broaden the absorption band, absorbing more UV

photons that is important for high sensitive device [133]. The unoptimized device showed a $D^* > 3 \times 10^{10}$ cmHz$^{1/2}$ W^{-1} at 2 V bias voltage under 0.01 mW cm^{-2} at the room temperature [133]. The study paved the way for developing large array, high performance, high uniformity, light weight and low cost UV FPA detectors [133]. These UV FPA detectors have important applications in astronomical research, environmental monitoring, forest fire prevention, medical analysis, and missile approach warning [133]. Figure 19 (a) shows the schematic illustration for fabrication of PFO/ZnO hybrid UV detector (b) the cross sectional SEM image of the device revealing the thicknesses of ITO, ZnO and PFO films are 161, 80 and 558 nm, respectively. Figure 20 shows the PFO/ZnO heterojunction may broaden the absorption band. The FWHMs of absorption peak for ZnO and PFO films are 42.0 and 67.5 nm respectively, their heterojunction gives 69.5 nm. These results were due to the fact that both junction components ZnO and PFO films can absorb UV photons efficiently, and the photogenerated electrons holes flow to ZnO PFO because of the electric potential difference between the two layers [133]. Figure 21 shows the PL for ZnO, PFO and their hybrid films. ZnO film showed a strong PL emission peak at 400 nm excited by various λ_{ex} ranging from 280 to 360 nm with a step of 20 nm [133]. Figure 22 shows the I-V characteristics for of the PFO/ZnO hybrid UV detector [133].

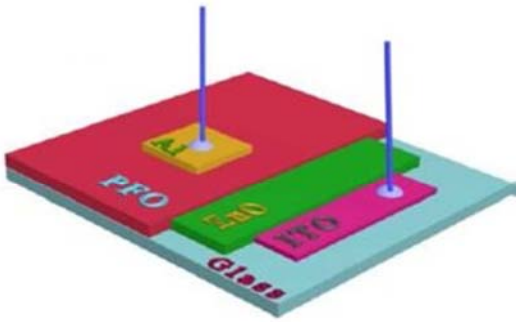

(a)

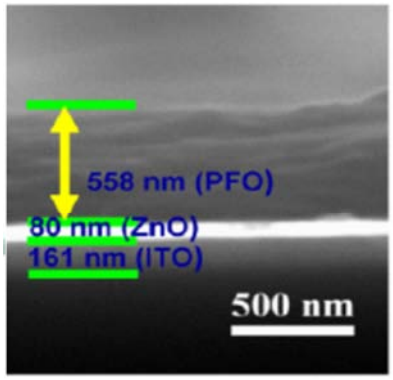

(b)

Figure 19. *(a) Schematic diagram of the PFO/ZnO hybrid UV detector (b) SEM image of the device [133].*

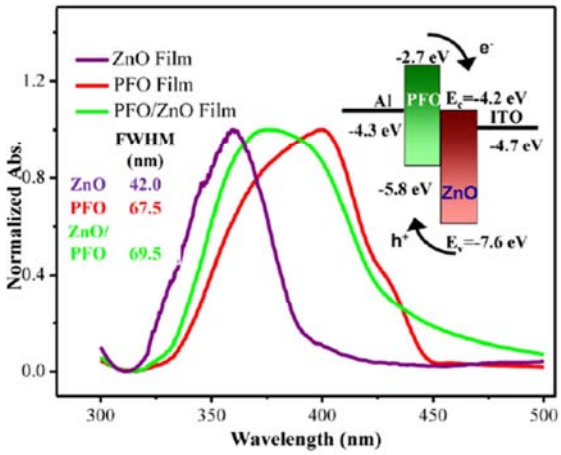

Figure 20. *Normalized UV-visible absorption spectra for ZnO, PFO, and PFO/ZnO films [133].*

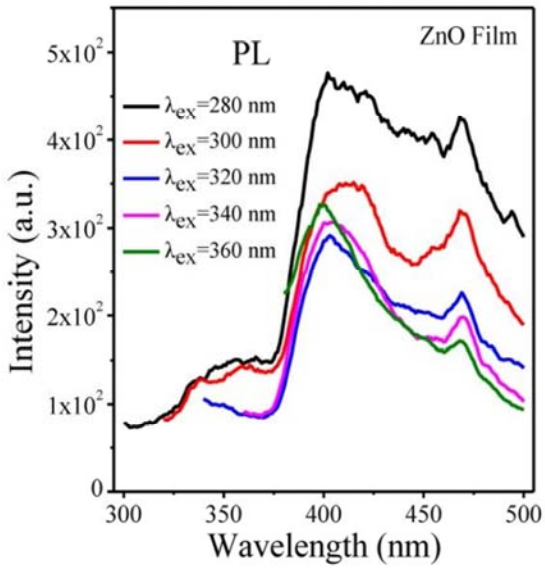

Figure 21. *PL spectra of ZnO film [133].*

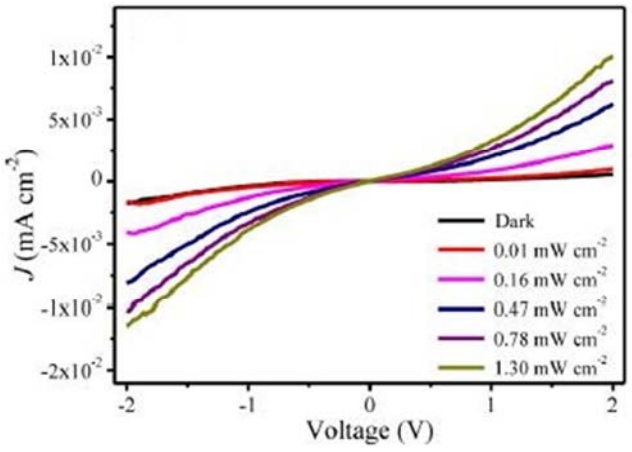

Figure 22. *I-V characteristics for the PFO/ZnO hybrid UV detector [133].*

The fabrication of the transparent bilayer InGaZnO:H/InGaZnO homojunction metal oxide thin film

transistors (TFT) was reported by Abliz et al. [134]. The bilayer structured device could enhance the mobility and instability issue of the indium gallium zinc oxide (InGaZnO) based TFTs [134]. The study's result showed that the fabricated devices exhibited high performances with the field effect mobility (μ_{FE}) of 55.3 cm $V^{-1}s^{-1}$, on/off current ratio (I_{on}/I_{off}) of 10^8, threshold voltage (V_{th}) of 0.7 V, and sub-threshold swing (SS) of 0.18 V/decade [134]. Besides, the bilayer InGaZnO:H/InGaZnO TFTs showed a good bias stress stability, where the threshold voltage shift (DV_{th}) of -0.8 V and 1.1 V under the negative gate bias stress (NBS) and positive gate bias stress (PBS) is much smaller than that of the single InGaZnO layer [134]. These characteristics were attributed to the InGaZnO:H ultrathin layer, which not only increases the carrier concentration (N_e) but also reduces the V_O of the defect states and the interfaces trap density [134]. Overall, the optimized bilayer InGaZnO:H/InGaZnO TFTs with μ_{FE} of above 50 cm $V^{-1}s^{-1}$ make realize competitive device performance and suitable switching behavior for the applications in future high resolution flat panel displays [134]. Figure 23 shows the schematic device structures of bilayer InGaZnO:H/InGaZnO based homojunction TFTs using silicon (Si) bottom gate [134]. Figure 24 (a) shows the optical bandgap (b) the near valence band edge peak (XPS) spectra of the pristine InGaZnO and hydrogenated InGaZnO:H 300 s films (c) the schematic band alignment energy diagrams indicate the relative energy position of the Fermi level, bandgap, conduction band, and valence band [134].

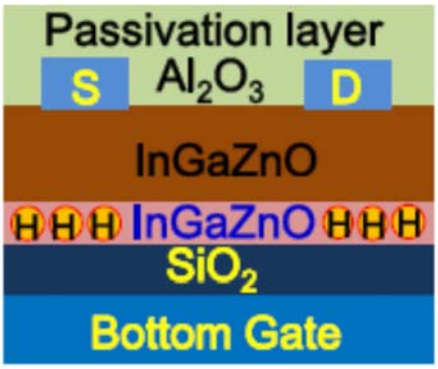

Figure 23. *Schematic device structures of bilayer InGaZnO:H/InGaZnO based homojunction TFTs using Si bottom gate [134].*

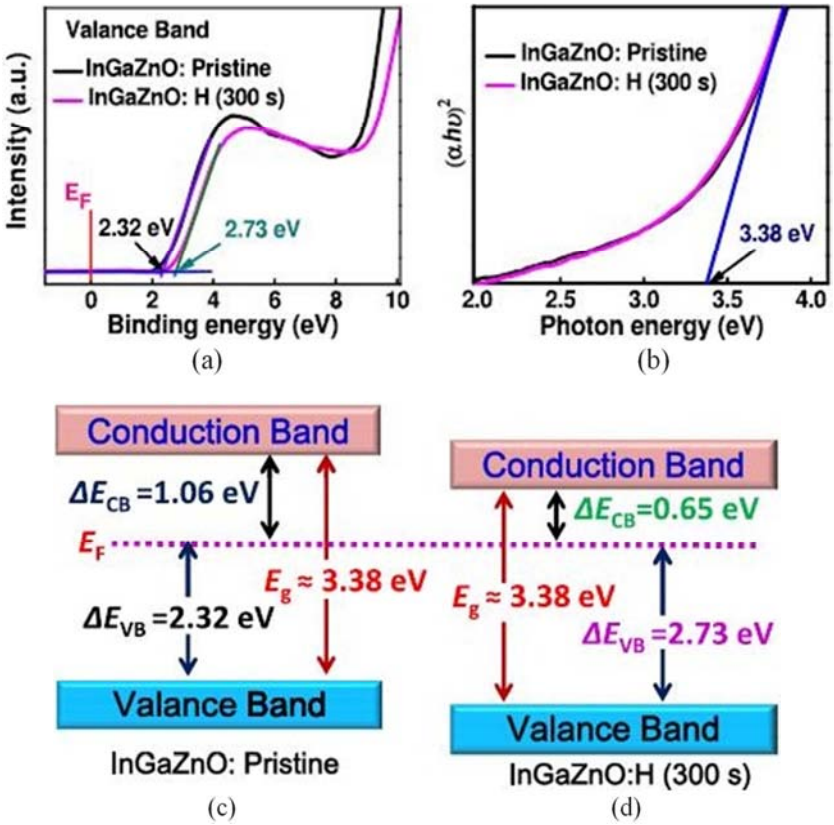

Figure 24. *(a) Optical bandgap (b) near valence band edge peak XPS spectra of the pristine InGaZnO and hydrogenated InGaZnO:H 300 s films (c) Schematic band alignment energy diagrams indicate the relative energy position of the Fermi level, bandgap, conduction band, and valence band (d) [134].*

The investigation of the promising materials for optoelectronic was demonstrated by introducing *n*-type inorganic material into conjugated polymer was reported by Azhar et al. [135]. The optical and the electrical of nanocomposite films based on poly [2-methoxy-5-2'-ethyl-hexyloxy-1,4-phenylene vinylene] (MEH-PPV) and ZnO nanostructured of various deposition layers 1 to 3 layers were investigated [135]. The MEH-PPV:ZnO nanocomposite films were deposited using spin coating technique [135]. The surface morphology nanocomposite films were characterized using the FESEM [135]. It was found that the thickness of the nanocomposite films increased as the deposition time increased [135]. The optical properties were measured using

PL spectroscope [135]. The PL spectra showed that two deposition layers has the highest intensity at the visible region green emission due to the high energy transfer from particles to the polymer [135]. The current density for two layers sample was due to the aggregation of the conjugated polymer chain hence form excited interchain exciton for the optical excitation [135]. That study provided a better performance and a suitable for optoelectronic device especially OLEDs application [135]. The study's results showed that the diameter size of the ZnO nanotetrapods in nanocomposite thin films increase when the layers increased [135]. These increases diameters might be due to the influence of the growth condition fluctuation on the crystal surface formation [135]. The PL spectra showed a prominent emission peak in the visible region indicate the high defect for 2 layers of the prepared nanocomposite thin films was found to increase with the deposition layers [135]. The resistance decreased as the deposition layer increased to 3 layers which was caused by the imperfection in the atomic lattice structure [135]. Figure 25 shows the FESEM images of the MEH-PPV: ZnO nanocomposite thin films at one layer. Figure 26 shows the PL of the MEH-PPV: ZnO nanocomposite thin films at different deposition layers [135].

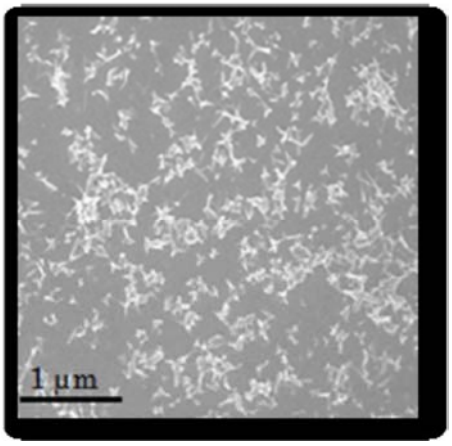

Figure 25. *FESEM images of MEH-PPV for ZnO nanocomposite thin films at one layer [135].*

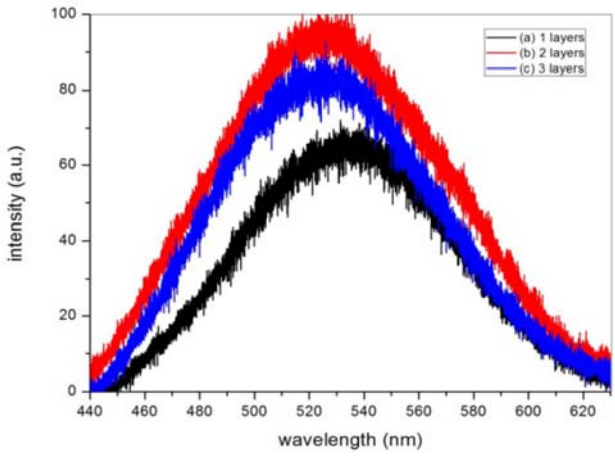

Figure 26. *PL of MEH-PPV: ZnO nanocomposite thin films at different deposition layers [135].*

6. GaN Based Devices

The organic/inorganic white light emitting F8T2 9,9-dioctylfluorene-co-bithiophene/GaN heterojunction was reported by Wu et al. [136]. The white light emission was produced by hybridizing the blue light 464 nm emitted from the GaN MQWs and the yellow/green light 500-650 nm emitted at the F8T2/*p*-GaN interface by EL [136]. The yellow/green light emission in the F8T2 layer was resulted from the carrier accumulation and the Frenkel excitons at the F8T2/*p*-GaN junction interface [136]. The study's results showed that the energy barrier and the large mobility discrepancy at the F8T2/*p*-GaN junction interface cause carriers accumulating in the F8T2 side near the F8T2/*p*-GaN interface [136]. The accumulated carriers at the F8T2/*p*-GaN interface form Frenkel excitons by Coulombic interaction [136]. Then, the Frenkel excitons recombine to radiate the yellow/green emission in the F8T2 layer. The international commission on illumination (CIE) coordinate of the white light emitted from the present device was at 0.28, 0.30, which was very close to the standard white light 0.33, 0.33 [136]. It was also found that the primary mechanism for this white light device was the EL based on the carrier accumulation and Frenkel excitons at the organic/inorganic F8T2/GaN interface and can allow further optimization of organic/inorganic optoelectronic devices [136]. The energy barrier and large mobility discrepancy at the F8T2/*p*-GaN junction interface would cause the carrier accumulation in the F8T2 side near the F8T2/*p*-GaN interface [136]. The strong coulombic interaction in F8T2 layer promotes the accumulated carriers form Frenkel excitons and radiate the yellow/green emission. Strikingly, there are two emission regions coexist in the hybrid structure to hybridize white light [136]. The white light emission was produced by hybridizing the blue light 464 nm emitted from the GaN MQWs with the yellow/green light 500-650 nm emitted at the F8T2/*p*-GaN interface by the EL [136]. The CIE coordinate of the white-light emission from the present device is at 0.28, 0.30, which is very close to the standard white light 0.33, 0.33 [136]. It was found that the F8T2/*p*-GaN interface creates a unique and an efficient carrier recombination and can combine with the traditional GaN light emitting diode for a potential extension of emission color range [136]. These results enhance further understanding on the characteristics of the carrier transport of hybrid interface [136]. It also provide an attractive white light EL device and extend the possibility of the large area hybrid white light GaN based emitting applications [136]. Figure 27 shows the schematic of the white light F8T2/GaN LED structure. Figure 28 shows the PL spectra of the F8T2, GaN MQWs, and F8T2/GaN MQWs structure with a 266 nm laser excitation source [136]. Figure 29 shows the EL spectra of the hybrid white light F8T2/GaN MQWs device under different applied forward voltage from 11 V to 15 V. The inset in the figure shows the EL spectra under a forward voltage of 11 V. Figure 30 shows the current density voltage luminance characteristics of the white-light F8T2/GaN MQWs device. The inset in the figure shows the power efficiency versus current density [136].

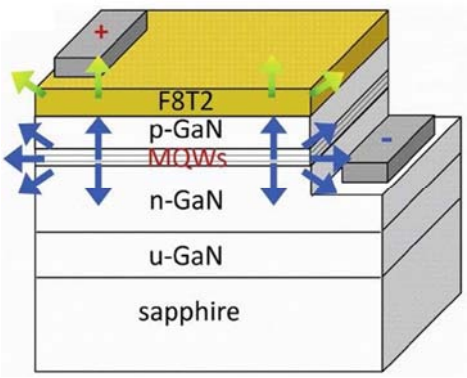

Figure 27. *Schematic diagram of the white-light F8T2/GaN LED structure [136].*

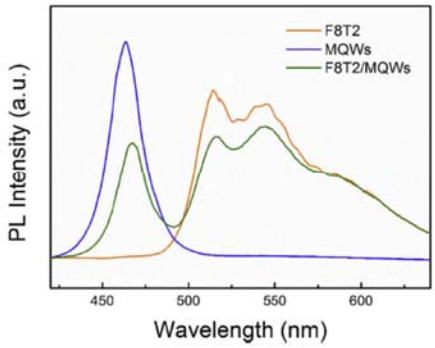

Figure 28. *PL spectra of F8T2, GaN MQWs, and F8T2/GaN MQWs structure with a 266 nm laser excitation source [136].*

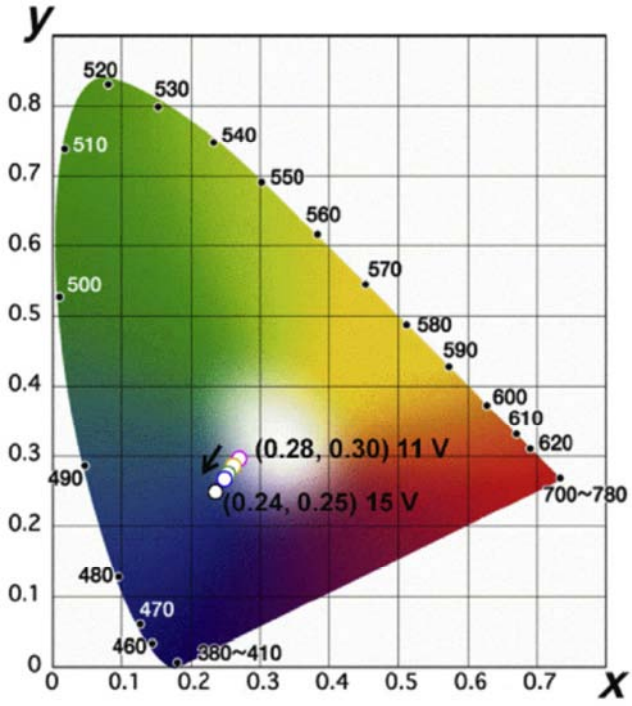

Figure 29. *EL spectra of the hybrid white light F8T2/GaN MQWs device under different applied forward voltage from 11 V to 15 V. The inset in EL spectra under a forward voltage of 11 V [136].*

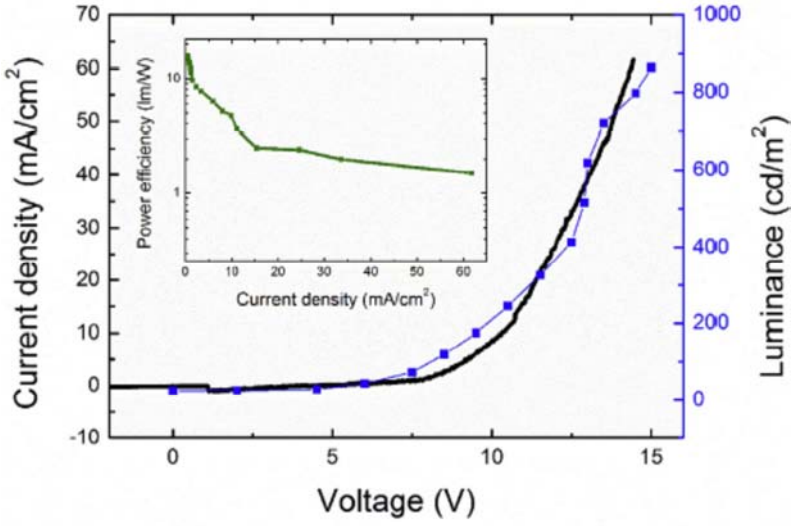

Figure 30. *Current density voltage luminance characteristics of the white light F8T2/GaN MQWs device. The inset shows the power efficiency versus current density [136].*

The organic/inorganic hybrid structures based on green polyfluorene F8BT and GaN (0001) nanorods grown by magnetron sputtering on Si (111) substrates was reported by Forsberg et al. [137]. In such nanorods, the stacking faults can form the periodic polymorphic QWs characterized by the bright luminescence [137]. The recombination rate for the stacking fault related emission increases in the presence of the polyfluorene film, which can be understood in terms of the Forster interaction mechanism [137]. The pumping efficiency of the nonradiative resonant energy transfer in the hybrids was estimated to be as high as 35% at low temperatures [137]. The study's results showed that an increased recombination rate of the stacking faults (SF) related transition in the polyfluorene presence at low temperatures [137]. That can be explained by the non-radiative resonance energy transfer (NRET) mechanism [137]. For the excitons confined in the SF QW like potential the requirement of the critical distance proximity can be fulfilled allowing, thus, the Forster interaction with dipoles in the polymer layer [137]. Figure 31 shows the scan electron microscopy (SEM) image of the

as-grown GaN nanorods sample on Si substrate with different lengths and diameters [137]. The SF presented in some nanorods are also schematically shown in the figure. Figure 32 shows the temperature dependent PL spectra measured at excitation power of 1 mW [137]. The spectra were normalized and shifted vertically for clarity [137]. The spectra taken for as-grown GaN nanorods and bare nanorods are shown by solid red lines, for nanorods covered by polyfluorene – by green dashed lines [137]. Figure 33 shows the temporal evolution of the recombination time (τ) for the SF PL line in the bare nanorods and after covering by polyfluorene [137].

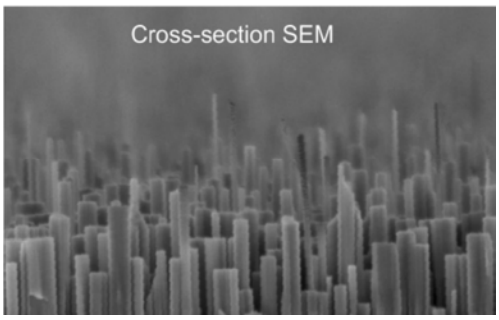

Figure 31. *SEM of GaN nanorods [137].*

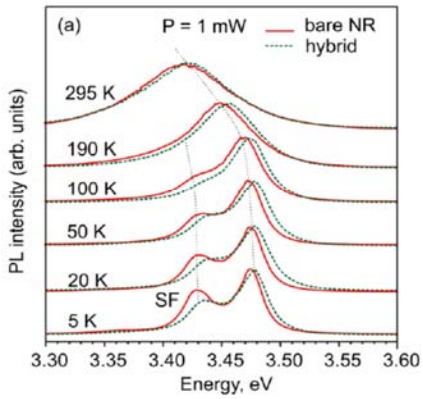

Figure 32. *Temperature dependent PL spectra measured at excitation power 1 mW [137].*

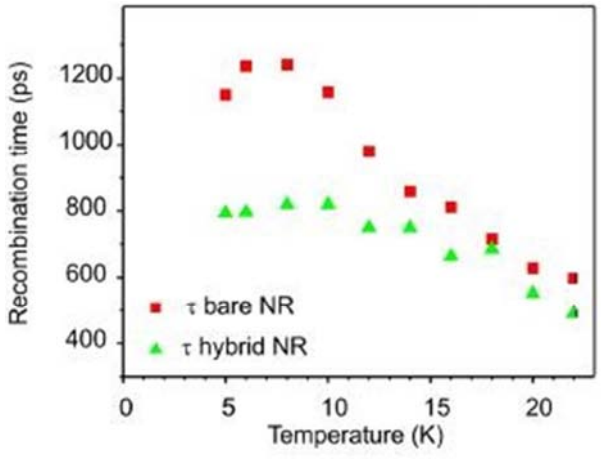

Figure 33. *Temporal evolution of the recombination time for the SF PL line in the bare nanorods and after covering by Polyfluorene [137].*

The hybrid optoelectronic device structures offer promising options for a wide range of properties [138]. The functioning of hybrid bilayer devices is largely determined by their interface [138]. The hybrid bilayer devices based on the wide bandgap GaN and low bandgap donor/acceptor polymers offer a unique combination and model interface systems for application in PDs. A systematic study of the optoelectronic properties [138], specifically the photocurrent as a function of voltage bias and incident wavelength, has been carried out for *n*-GaN/polymer bilayer structures was reported by Kumar et al. [138]. The study's results showed that the charge transport was strongly affected by the interface charge trapping and the polarization effects which was introduced by the nitride surface. The *n*-GaN/donor polymer hybrid system utilizes the 450-650 nm defect state emission of *n*-GaN, which was advantageous since this emission was reabsorbed by the donor polymer resulting in an enhanced photocurrent, significantly increasing the UV detection capacity [138]. An important issue to be addressed for improving the detectivity of *n*-GaN/donor polymer-based hybrid diodes was to modify the hybrid interface, such that any trapping dominated influence or polarization related effects on charge transport and photogeneration may be controlled [138]. An increase in the responsivity for the reverse bias as well as the forward bias has been observed [138]. The maximum applied reverse bias was strongly limited by the reverse leakage current [138]. The high photodetection efficiency of nitride polymer hybrid devices can be achieved by modifying the interface to reduce the magnitude of leakage current and other losses due to the recombination [138]. Figure 34 shows the schematics of the *n*-GaN/D hybrid device structure. Figure 35 shows the XRD has been utilized to probe the ordering present in the polymer films coated on GaN. Figure 36 shows the photocurrent response from *n*-GaN/PBTTT-C14 and *n*-GaN/P3HT under white light illumination 100 mW/cm^2. The inset shows the dark and light I-V characteristics for *n*-GaN/N2200 diode [138].

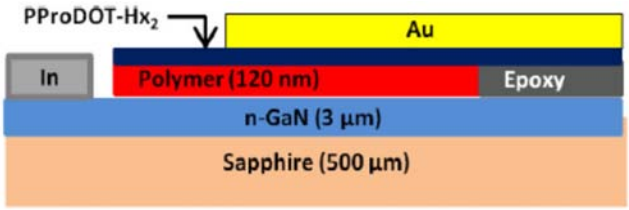

Figure 34. *Schematic of n-GaN/D hybrid diode structure [138].*

The hybrid device that combines the properties of organic/inorganic semiconductors was fabricated and reported by Shin et al. [139]. The device incorporated poly [2-methoxy-5-2-ethylhexyloxy-1,4-henylenevinylene] (MEH-PPV) and poly 3,4-ethylenedioxythiophene: poly styrene sulfonate (PEDOT: PSS) as some organic polymers and GaN nanoneedles as an inorganic semiconductor [139]. The layers of the two polymers were spin coated onto the GaN nanoneedles [139]. The one peak in the EL originated from the MEH-PPV layer owing to the different potential barriers of electrons and holes at its interface with the GaN nanoneedles

[139]. However, the PL spectrum showed peaks due to both GaN nanoneedles and MEH-PPV [139]. Such hybrid structures, suitably developed, might be able to improve the efficiency of optoelectronic devices [139]. Figure 37 shows the FESEM images of MEH-PPV layer on GAN nanoneedles. Figure 38 shows the hybrid LED structure of GaN [139]. Figure 39 shows the I-V characteristics of the MEH-PPV/PEDOT:PSS layer on GaN nanoneedles and semi-logarithmic plot of I-V characteristics inset [139].

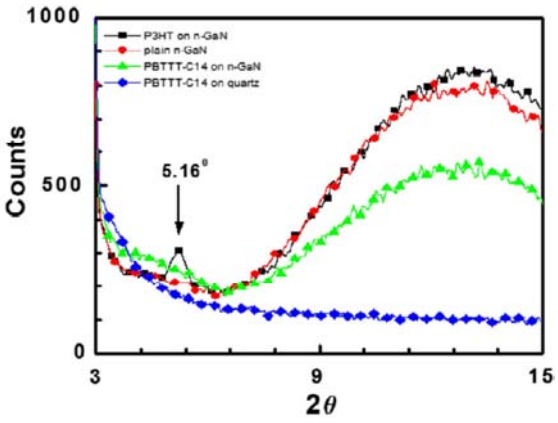

Figure 35. *XRD for P3HT on n-GaN, Plane n-GaN, PBTTT-C14 on n-GaN and PBTTT-C14 on quartz [138].*

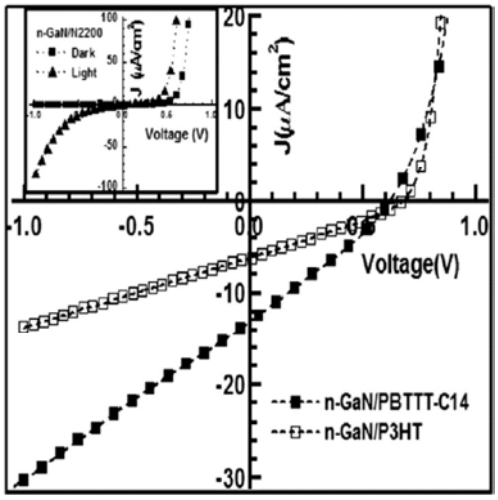

Figure 36. *Photocurrent response from n-GaN/PBTTT-C14 and n-GaN/P3HT under white light illumination 100 mW/cm^2. Inset shows the dark and light I-V characteristics for n-GaN/N2200 diode [138].*

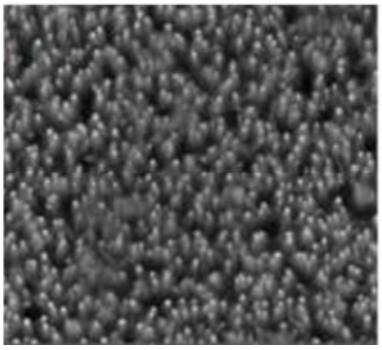

Figure 37. *FESEM images: MEH-PPV layer on GaN nanoneedles [139].*

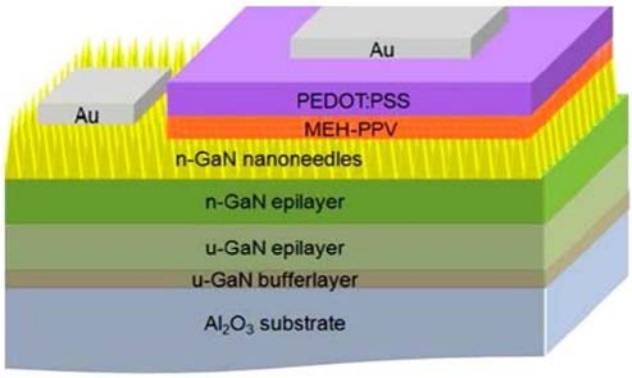

Figure 38. *Hybrid LED structure of GaN [139].*

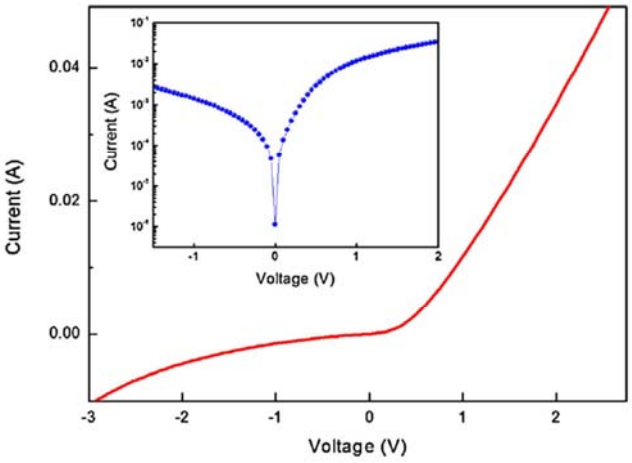

Figure 39. *I-V characteristics of the MEH-PPV/PEDOT: PSS layer on GaN nanoneedles and semi-logarithmic plot of I-V characteristics inset [139].*

The organic/inorganic hybrid hetero structure for optoelectronic device and applications was reported by Shin et al. [85]. The structure was fabricated using inorganic material consisting of GaN nanoneedles and the hole conducting polymer PEDOT:PSS [85]. The PEDOT:PSS layer with a thickness of 50 nm was deposited using the spin coating on GaN nanoneedles grown using an hydride vapor phase epitaxial (HVPE) system [85]. The GaN nanoneedle/PEDOT:PSS structure showed a broader, shifted emission peak in the PL measurements compared with the GaN epilayer/PEDOT: PSS structure, as well as a lower turn-on voltage when the I-V characteristics were measured [85]. The PL peaks for the GaN nanoneedle PEDOT:PSS and GaN epilayer/PEDOT:PSS structures were due only to the GaN materials, regardless of the PEDOP:PSS peak [85]. The broadened and shifted PL peak for the GaN nanoneedle/PEDOT:PSS structure was presumed to result from the various magnitudes of the stresses in differently strained domains within the nanoneedles [85]. That led to the low turn-on voltage observed in the I-V characteristics, which showed a stable and a well behaved rectification [85]. The study's results showed that the GaN nanoneedle/PEDOT:PSS heterojunction structures reduce the importance of achieving the *p*-type doping of GaN nanostructures, and hold strong potential for GaN based polymer optoelectronic devices [85]. Figure 40 shows the schematic diagram of the GaN

nanoneedle/PEDOT:PSS hybrid heterojunction structure. Figure 41 shows the FESEM images of the GaN hybrid structure. Figure 42 shows the PL spectra for the present GaN nanoneedle/PEDOT: PSS and GaN epilayer/PEDOT: PSS structures, measured at room temperature. A strong narrow PL peak and a yellow luminescence band were observed for the GaN epilayer/PEDOT: PSS, and a broad blue emission band was observed for the GaN nanoneedle/PEDOT: PSS structure [85].

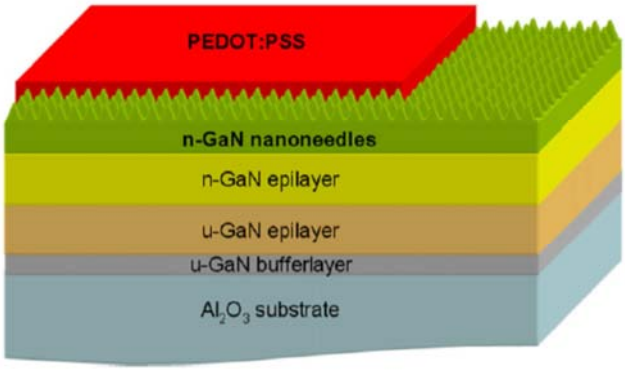

Figure 40. *Schematic diagram of the GaN nanoneedle/PEDOT:PSS hybrid heterojunction structure [85].*

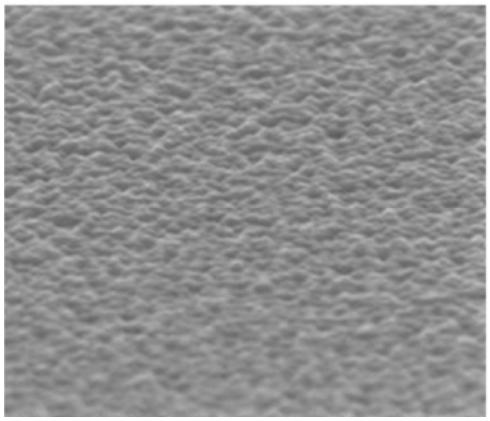

Figure 41. *FESEM image of GaN nanoneedles [85].*

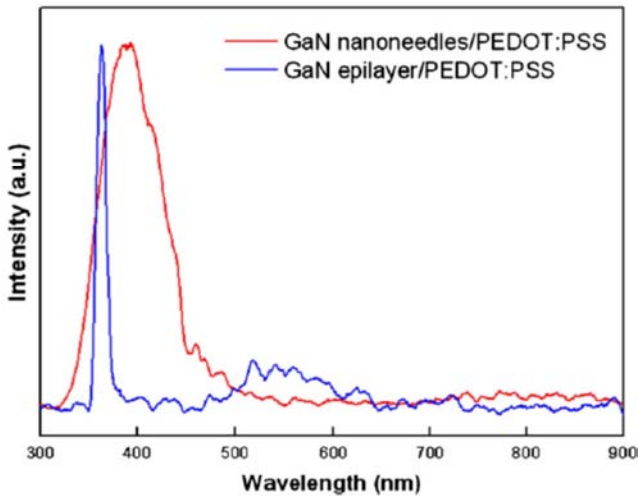

Figure 42. *PL spectra for GaN nanoneedle/PEDOT:PSS and GaN epilayer/PEDOT:PSS heterojunction structures [85]. 7. Conclusion.*

The recent development of the GaN/ZnO hybrid-based materials and devices has been reviewed. GaN/ZnO hybrid materials are forming a very encouraging material system due to the easy fabrication, high flexibility, superior electrical, optical properties, low cost, easy process ability, and large scale manufacturing which enables to offer improved functionalities to nano-optoelectronics including OSCs. Regardless of the developments in that area, many issues still need to be more investigated. The issue of the highly efficient OSCs using nanoscale materials is still very challenging. The utilization of GaN and ZnO materials is promising to increase the OSCs efficiency. Moreover, the efficiency can be further improved by developing a powerful photosensitizer with broad spectral range and higher molar extinction coefficient than the existing sensitizers, improving the open circuit voltage which is the difference between the quasi fermi level in semiconductor and redox couple in electrolyte, the use of suitable electrolyte to boost the open circuit voltage value for a particular semiconductor. Moreover, the efficiency of the GaN/ZnO based devices can be further improved by the thermal annealing treatment. The annealing treatment helps to restore the crystallization of the GaN/ZnO films. Consequently, it improves the device performance and removes the defects. Moreover, the introducing of the buffer layer as an interfacial layer between the active layer and the electrode plays a crucial role in the GaN/ZnO based devices, as they may impact the device polarity by selectively transporting the charge carriers, energy barrier at the contact interface, light propagation and distribution, electrode surface affinity and active layer morphology. Moreover, doping of the GaN/ZnO devices helps to passivate the defects, reduce the charge carrier recombination, increase the charge carrier concentration and thus increase the interlayer conductivity. The major drawback of the GaN/ZnO inorganic devices is they possesses lesser light absorptivity than organic materials. Therefore, inorganic semiconductors require more quantity of absorbing layers which makes them thicker. Also, to achieve better efficiency, purity of inorganic semiconductors is most important factor which increases the cost with increase in the purity. Furthermore, a high quality GaN/ZnO based devices with hetero-interfaces layers in the architecture of PSCs are essential. These hetero-interfaces can be improved by introducing a buffer layer which improves the structural stability of the GaN/ZnO thin films. Finally, the GaN/ZnO based devices performance can be improved by optimizing the deposition and the thin film properties including the crystalline structures, the film quality, the growth method, the film morphology. Moreover, the presence of the residual affects the device stability and cause the degradation of the device performance under illumination.

References

[1] I. Khan, S. Khan, R. Nongjai, H. Ahmed, and W. Khan, "Hydrothermal synthesis of zinc oxide powders with controllable morphology," Optical Materials 35, 1189-1193 (2013).

[2] L. Znaidi, "Sol-gel deposited ZnO thin films: A review," Materials Science and Engineering: B 174, 18-30 (2010).

[3] H. Xu, H. Wang, Y. Zhang, W. He, M. Zhu, B. Wang, and H. Yan, "Structural and optical properties of gel-combustion synthesized Zr doped ZnO nanoparticles," Ceramics International 30, 93-97 (2004).

[4] Z. Wang, "Zinc oxide nanostructures: growth, properties and applications," Journal of Physics: Condensed Matter 16, R829 (2004).

[5] A. Djurisic, A. Ng, and X. Chen, "ZnO nanostructures for optoelectronics: Material properties and device applications," Progress in Quantum Electronics 34, 191-259 (2010).

[6] Z. Wang and J. Song, "Piezoelectric nanogenerators based on Zinc Oxide nanowire arrays," Science 312, 242-246 (2006).

[7] P. Wu, J. Zhang, J. Lu, X. Li, C. Wu, R. Sun, L. Feng, Q. Jiang, B. Lu, X. Pan, and Z. Ye, "Instability induced by ultraviolet light in ZnO thin-film transistors," IEEE Transactions on Electron Devices, 61, 1431-1435 (2014).

[8] L. Li, Y. Zhang, L. Yan, J. Jiang, X. Han, G. Deng, C. Chi, and J. Song, "n-ZnO/p-GaN heterojunction light-emitting diodes featuring a buried polarization-induced tunneling junction," AIP Adances 6, 125204 (2016).

[9] L. Sin, M. Arshad, M. Fathil, R. Adzhri, M. Nuzaihan, A. Ruslinda, S. Gopinath, and U. Hashim, "Zinc oxide interdigitated electrode for biosensor application," AIP Conference Proceedings 1733, 020075 (2016).

[10] Y. Yuliah, A. Bahtiar, Fitrilawati, and R. Siregar, "The optical bandgap investigation of PVP-capped ZnO nanoparticles synthesized by sol-gel method," AIP Conference Proceedings 1712, 050018 (2016).

[11] R. Konenkamp, R. Word, and C. Schegel, "Vertical nanowire light-emitting diode," Applied Physics Letters 85, 6004-6006 (2004).

[12] S. Mckinstry and P. Marult, "Thin film piezoelectrics for MEMS," Journal of Electroceramics 12, 7-17 (2004).

[13] Y. Ushio, M. Miyayama and H. Yanagida, "Effects of interface states on gas sensing properties of a CuO/ZnO thin film heterojunction," Sensors and Actuators B: Chemical 17, 221-226 (1994).

[14] H. Harima, "Raman studies on spintronics materials based on wide bandgap semiconductors," Journal of Physics: Condensed Matter 16, S5653-S5660 (2004).

[15] J. Xiang, P. Zhu, Y. Masuda, M. Okuya, S. Kaneko, and K. Koumoto, "Flexible solar cell from Zinc Oxide nanocrystalline sheets self assembled by an In-Situ electrodeposition process," Journal of Nanoscience and Nanotechnology 6, 1797-1801 (2006).

[16] U. Khachar, P. Solanki, R. Choudhary, D. Phase, V. Ganesan, and D. Kuberkar, "Room temperature positive magnetoresistance and field effect studies of manganite-based heterostructure," Applied Physics A 108, 733-738 (2012).

[17] J. Roh, H. Kim, M. Park, J. Kwak, and C. Lee, "Improved electron injection in all solution processed n-type organic field effect transistors with an inkjet printed *ZnO* electron injection layer," Applied Surface Science 420, 100-104 (2017).

[18] M. Zhang, H. Zhang, L. Li, K. Tuokedaerhan, and Z. Jia, "Er-enhanced humidity sensing performance in black *ZnO* based *sensor*," Journal of Alloys and Compounds 744, 364-369 (2018).

[19] L. Zhu, and W. Zeng, "Room-*temperature* gas sensing of *ZnO* based gas *sensor:* A review," *Sensors* and Actuators A: Physical 267, 242-261 (2017).

[20] F. Boccuzzi, A. Chiorino, S. Tsubota, and M. Haruta, "An IR study of CO-sensing mechanism on Au/ZnO," Sensors and Actuators B: Chemical 25, 540-543 (1995).

[21] J. Singh, S. Patil, M. More, D. Joag, R. Tiwari, and O. Srivastava, "Formation of aligned ZnO nanorods on self grown ZnO template and its enhanced field emission characteristics," Applied Surface Science 256, 6157-6153 (2010).

[22] M. Alvi, A. Al-Ghamdi, and M. Husain, "Field emission studies of CNTs/ZnO nanostructured thin films for display devices," Physica B: Condensed Matterials 521, 312-316 (2017).

[23] C. Lao, P. Gao, R. Yang, Y. Zhang, Y. Dai and Z. Wang, "Formation of double side teethed nanocombs of ZnO and self catalysis of Zn terminated polar surface," Chemical Physics Letters 417, 358-362 (2006).

[24] J. Zhou, X. Wu, D. Xiao, M. Zhuo, H. Jin, J. Luo, and Y. Fu, "Deposition of aluminum doped ZnO as electrode for transparent ZnO/glass surface acoustic wave devices," Surface and Coatings Technology 320, 39-46 (2017).

[25] T. Majumdera, S. Dhara, P. Chakrabortya, K. Debnathb, and S. Mondala, "Advantages of ZnO nanotaper photoanodes in photoelectrochemical cells and graphene quantum dot sensitized solar cell applications," Journal of Electroanalytical Chemistry 813, 92-101 (2018).

[26] S. Arya, S. Saha, J. Ramirez-Vick, V. Gupta, S. Bhansali, and S. Singh, "Recent advances in ZnO nanostructures and thin films for biosensor applications: Review," Analytica Chimica Acta 737, 1-21 (2012).

[27] G. Yu, J. Gao, J. Hummenlen, A. Heeger, and F. Wudl, "Polymer photovoltaic cells: enhanced efficiencies via a network of internal donor-acceptor heterojunctions," Science 270, 1789-1791 (1995).

[28] S. Shaheen, C. Brabec, N. Sariciftci, F. Padinger, T. Fromherz, and J. Hummenlen, "2.5% efficient organic plastic solar cells," Applied Physics Letters 78, 841-844 (2001).

[29] L. Nulhakim and H. Makino, "Change of scattering mechanism and annealing out of defects on Ga-doped ZnO films deposited by radio frequency magnetron sputtering," Journal of Applied Physics 119, 235302 (2016).

[30] D. Montenegro, A. Souissi, C. Tomas, V. Sanjose, and V. Sallet, "Morphology transitions in ZnO nanorods grown by MOCVD," Journal of Crystal Growth 359, 122-128 (2012).

[31] N. Oleynik, M. Adam, A. Krtschil, J. Blasing, A. Dadgar, F. Bertram, D. Forster, A. Diez, A. Greiling, M. Seip, J. Christen, and A. Krost, "Metalorganic chemical vapor phase deposition of ZnO with different O-precursors," Journal of Crystal Growth 248, 14-19 (2003).

[32] V. Litovchenko, A. Evtukh, and A. Grygoriev, "Characterization of GaN nanostructures by electron field and photo field emission," Opto-Electronics Review 25, 251-262 (2017).

[33] T. Honda, K. Yoshioka, "Fabrication of GaN‐based Schottky-type light-emitting diodes for micropixels in flat‐panel displays," 7th International Conference on Nitride Semiconductors (ICNS-7) 5, 2225-2227 (2008).

[34] X. Zheng, M. Guidry, H. Li, E. Ahmadi, K. Hestroffer, B. Romanczyk, S. Wienecke, S. Keller, and U. Mishra, "N-polar GaN MIS-HEMTs on sapphire with high combination of power gain cutoff frequency and three-terminal breakdown voltage," IEEE Electronic Device Letters 37, 77-80 (2016).

[35] H. Chiu, S. Chen, J. Chiu, B. Li, H. Wang, L. Peng, H. Wang, and K. Hsueh, "AlGaN/GaN Schottky barrier diodes on silicon substrates with various Fe doping concentrations in the buffer layers," Microelectronics Reliability 83, 238-241 (2018).

[36] S. Mohammad and H. Morkoc, "Progress and prospects of group-III nitride semiconductors," Progress in Quantum Electronics 20, 361-525 (1996).

[37] D. Zhu, D. Wallis, and C. Humphreys, "Prospects of III-nitride optoelectronics grown on Si," Reports on Progress in Physics 76, 106501 (2013).

[38] A. Fletcher and D. Nirmal, "A survey of gallium nitride HEMT for RF and high power applications," Superlattices and Microstructures 109, 519-537 (2017).

[39] B. Baliga, "Gallium nitride devices for power electronic applications," Semiconductor Science and Technology 28, 074011 (2013).

[40] S. Pearton and F. Ren, "GaN electronics," Advanced Materials 12, 1571-1580 (2000).

[41] N. Fu, E. Li, Z. Cui, D. Ma, W. Wang, Y. Zhang, S. Song, and J. Lin, "The electronic properties of phosphorus doped GaN nanowires from first principle calculations," Journal of Alloys Compound 596, 92-97 (2014).

[42] Y. Wang, R. Wang, Y. Li, Y. Zhang, M. Zhu, B. Wang, and H. Yan, "From powder to nanowire: a simple and environmentally friendly strategy for optical and electrical GaN nanowire films," CrystEngComm 15, 1626-1634 (2013).

[43] S. Pearton, B. Kang, S. Kim, F. Ren, B. Gila, C. Abernathy, J. Lin, and S. Chu, "GaN based diodes and transistors for chemical, gas, biological and pressure sensing," Journal of Physics: Condensed Matter 16, R961-R994 (2004).

[44] M. Neuberger, T. Zimmermann, P. Benkart, M. Kunze, I. Daumiller, A. Dadgar, A. Krost, and E. Kohn, "GaN based piezo sensors," Device Research Conference 4, 5-46 (2004).

[45] B. Kang, J. Kim, S. Jang, F. Ren, J. Johnson, R. Therrien, P. Rajagopal, J. Roberts, E. Piner, K. Linthicum, S. Chu, K. Baik, B. Gila, C. Abernathy, and S. Pearton, "Capacitance pressure sensor based on GaN high electron mobility transistor on Si membrane," Applied Physics Letters 86, 253502 (2005).

[46] S. Pearton, F. Ren, E. Patrick, M. Law, and A. Polyakov, "Review-Ionizing radiation damage effects on GaN devices," ECS Journal of Solid State Science and Technology 5, Q35-Q60 (2016).

[47] S. Kako, C. Santori, K. Hoshino, S. Gotzinger, Y. Yamamoto, and Y. Arakawa, "A gallium nitride single-photon source operating at 200 K," Nature Materials 5, 887-892 (2006).

[48] S. DenBaars, D. Feezell, K. Kelchner, S. Pimputkar, C. Pan, C. Yen, S. Tanaka, Y. Zhao, N. Pfaff, R. Farrell, M. Iza, S. Keller, U. Mishra, J. Speck, and S. Nakamura, "Development of gallium nitride based light emitting diodes (LEDs) and laser diodes for energy efficient lighting and displays," Acta Materialia 61, 945-951 (2013).

[49] M. Zhang, Q. Jiang, F. Hou, Z. Wang, and G. Pan, "Fabrication of high aspect ratio gallium nitride nanostructures by photochemical etching for enhanced photocurrent and photoluminescence property," Scripta Materialia 146, 115-118 (2018).

[50] Y. Lin, W. Liu, C. Chang, C. Chung, and Y. Chen, "Internal quantum efficiency enhancement by relieving compressive stress of GaN based LED," IEEE Photonics Technology Letters 26, 1793-1796 (2014).

[51] N. Park, M. Oh, Y. Na, W. Cheong, and H. Kim, "Sputter deposition of Sn-doped ZnO/Ag/Sn-doped ZnO transparent contact layer for GaN LED applications," Materials Letters 180, 72-76 (2016).

[52] C. Chen, W. Chen, C. Chang, Y. Lee, and W. Liu, "Implementation of light extraction improvements of GaN based light emitting diodes with specific textured sidewalls," Optics and Laser Technology 101, 172-176 (2018).

[53] X. He, D. Zhao, D. Jiang, J. Zhu, P. Chen, Z. Liu, L. Le, J. Yang, X. Li, and J. Liu, "GaN high electron mobility transistors with AlInN back barriers," Journal of Alloys and Compounds 662, 16-19 (2016).

[54] M. Khan, J. Kkuznia, D. Olson, and M. Blasingame, "Schottky barrier photodetector based on Mg‐doped p‐type GaN films," Applied Physics Letters 63, 2455 (1993).

[55] Y. Su, Y. Chiou, F. Juang, S. Chang, "GaN and InGaN metal semiconductor metal photodetectors with different Schottky contact metals," Japanese Journal of Applied Physics 40, 2996 (2001).

[56] J. Seo, C. Caneau, R. Bhat, and I. Adesida, "Application of indium tin oxide with improved transmittance at 1.3 mu for MSM photodetectors," IEEE Photonics Technology Letters 5, 1313-1315 (1993).

[57] L. Ravikiran, K. Radhakrishnan, N. Dharmarasu, M. Agrawal, Z. Wang, A. Bruno, C. Soci, T. Lihuang, and A. Siong, "Responsivity drop due to conductance modulation in GaN metal semiconductor metal Schottky based UV photodetectors on Si (111)," Semiconductor Science and Technology 31, 095003 (2016).

[58] S. Yoon, J. Lee, and T. Seong, "Inhomogeneity of barrier heights of transparent Ag/ITO Schottky contacts on n-type GaN annealed at different temperatures," Journal of Alloys and Compounds 742, 66-71 (2018).

[59] T. Flack, B. Pushpakaran, and S. Bayne, "GaN technology for power electronic applications: a review," Journal of Electronic Materials 45, 2673 (2016).

[60] T. Wang, B. Wang, A. Haque, M. Snure, E. Heller, and N. Glavin, "Mechanical stress effects on electrical breakdown of freestanding GaN thin films," Microelectronics Reliability 81, 181-185 (2018).

[61] S. Ghosh, S. Dinara, M. Mahata, S. Das, P. Mukhopadhyay, S. Jana, and D. Biswas, "On the different origins of electrical parameter degradation in reverse bias stressed AlGaN/GaN HEMTs," Physica Status Solidi A 213, 1559-1563 (2016).

[62] R. Long, A. Hazeghi, M. Gunji, Y. Nishi, and P. McIntyre, "Temperature dependent capacitance voltage analysis of defects in Al_2O_3 gate dielectric stacks on GaN," Applied Physics Letters 101, 1-5 (2012).

[63] A. Chakraborty, S. Ghosh, P. Mukhopadhyay, S. Das, A. Bag, and D. Biswas, "Effect of trapped charge in AlGaN/GaN and AlGaN/InGaN/GaN heterostructure by temperature dependent threshold voltage analysis," Superlattices and Microstructures 113, 147-152 (2018).

[64] M. Reshchikov, G. Yi, and B. Weasels, "Behavior of 2.8- and 3.2-eV photoluminescence bands in Mg-doped GaN at different temperatures and excitation densities," Physics Review B 59, 13176-13183 (1999).

[65] H. Cho, J. Lee, G. Yang, and C. Kim, "Formation mechanism of V defects in the InGaN/GaN multiple quantum wells grown on GaN layers with low threading dislocation density," Applied Physics Letters 79, 215-217 (2001).

[66] R. Colby, Z. Liang, I. Wildeson, D. Ewoldt, T. Sands, R. Garcia, and E. Stach, "Dislocation filtering in GaN nanostructures," Nano 10, 1568-1573 (2010).

[67] C. Xu, S. Chung, M. Kim, D. E. Kim, B. Chon, S. Hong, and T. Joo, "Doping of Si into GaN nanowires and optical properties of resulting composites," Journal of Nanoscience and Nanotechnology 5, 530 (2005).

[68] J. Arbiol, S. Estrad, J. Prades, A. Cierea, F. Furtmayr, C. Stark, A. Laufer, M. Stutzmann, M. Eickhoff, M. Gass, A. Bleloch, F. Peir, and J. Morante, "Triplet win domains in Mg doped GaN wurtzite nanowires: structural and electronic properties of this zinc blende like stacking," Nanotechnology 20, 145704 (2009).

[69] R. Wu, G. Peng, L. Liu, Y. Feng, Z. Huang, and Q. Wu, "Cu-doped GaN: a dilute magnetic semiconductor from first principles study," Applied Physics Letters 89, 062505 (2006).

[70] K. Stamplecoskie, L. Ju, S. Farvid, and P. Radovanovic, "General control of transition metal doped GaN nanowire growth: toward understanding the mechanism of dopant incorporation," Nano Letters 8, 2674-2681 (2008).

[71] S. Zhou, "Near UV photoluminescence of Hg-doped GaN nanowires," Physica E: Low-dimensional Systems and Nanostructures 33, 394-397 (2006).

[72] S. Zhou, "Fabrication and PL of Al-doped gallium nitride nanowires," Physics Letters 357, 374-377 (2006).

[73] E. Li, B. Wu, S. Lv, Z. Cui, D. Ma, and W. Shi, "Field emission properties of Ge-doped GaN nanowires," Journal of Alloys and Compounds 681, 324-329 (2016).

[74] Z. Cui, X. Ke, E. Li, and T. Liu, "Electronic and optical properties of titanium doped GaN nanowires," Materials and Design 96, 409-415 (2016).

[75] E. Li, J. Yan, D. Ma, Z. Cui, and Q. Qi, "Synthesis and field emission performance for P-doped GaN NWs," Superlattices and Microstructures 115, 53-58 (2018).

[76] S. Chang, R. Chuang, S. Chang, Y. Chiou, and C. Lu, "MBE n-ZnO/MOCVD p-GaN heterojunction light emitting diode," Thin Solid Films 517, 5054-5056 (2009).

[77] F. Tuomisto, D. Look, and G. Farlow, "Defect studies in electron irradiated ZnO and GaN," Physica B 401-402, 604-608 (2007).

[78] F. Tuomisto, "Vacancy profiles and clustering in light ion implanted GaN and ZnO," Applied Surface Science 255, 54-57 (2008).

[79] E. Wendler, W. Wesch, A. Yu. Azarov, N. Catarino, A. Redondo-Cubero, E. Alves, and K. Lorenz, "Comparison of low and room temperature damage formation in Ar ion implanted GaN and ZnO," Nuclear Instruments and Methods in Physics Research B 307, 394-398 (2013).

[80] S. Galagali, N. Sankeshwar, and B. Mulimani, "Thermoelectric transport in ZnO and GaN nanowires," Journal of Physics and Chemistry of Solids 83, 8-17 (2015).

[81] D. Reynolds, D. Look, and B. Jogai, "Optically pumped ultraviolet lasing from ZnO," Solid State Communications 99, 873 (1996).

[82] D. Bagnall, Y. Chen, Z. Zhu, T. Yao, S. Koyama, M. Shen, and T. Goto, "Optically pumped lasing of ZnO at room temperature," Applied Physics Letters 70, 873 (1997).

[83] S. Lee and D. Kim, "Characteristics of ZnO/GaN heterostructure formed on GaN substrate by sputtering deposition of ZnO," Materials Science and Engineering B 137, 80-84 (2007).

[84] A. Wadeasa, O. Nur, and M. Willander, "The effect of the interlayer design on the electroluminescence and electrical properties of n-ZnO nanorod/p-type blended polymer hybrid light emitting diodes," Nanotechnology 20, 80-84 (2009).

[85] M. Shin, M. Kim, G. Lee, H. Ahn, S. Yi, and D. Ha, "A GaN nanoneedle inorganic/organic heterojunction structure for optoelectronic devices," Materials Letters 91, 191-194 (2013).

[86] P. Reyes, C. Ku, Z. Duan, Y. Xu, E. Garfunkel, and Y. Lu, "Reduction of persistent photoconductivity in ZnO thin film transistor based UV photodetector," Applied Physics Letters 101, 031118 (2012).

[87] S. Yang, S. Tongay, S. Li, J. Xia, J. Wu, J. Li, E. Garfunkel, and Y. Lu, "Environmentally stable/self-powered ultraviolet photodetectors with high sensitivity," Applied Physics Letters 103, 143503 (2013).

[88] X. Li, W. Liu, P. Li, J. Song, Y. An, J. Shen, S. Wang, and D. Guo, " A self powered nano-photodetector based on PFH/ZnO nanorods organic/inorganic heterojunction," Results in Physics 8, 468-472 (2018).

[89] Z. Wei, H. Almakrami, G. Lin, E. Agar, and F. Liu, "An organic-inorganic hybrid photoelectrochemical storage cell for improved solar energy storage," Electrochimica Acta 263, 570-575 (2018).

[90] Y. Vaynzof, D. Kabra, L. Zhao, P. Ho, A. Wee, and R. Friend, "Improved photoinduced charge carriers separation in organic-inorganic hybrid photovoltaic devices," Applied Physics Letters 97, 033309 (2010).

[91] J. Chang, J. Rhee, S. Im, Y. Lee, H. Kim, S. Seok, M. Nazeeruddin, and M. Gratzel, "High performance nanostructured Inorganic-Organic heterojunction solar cells," Nano Letters 10, 2609 (2010).

[92] V. Agranovich, Y. Gartstein, and M. Litinskaya, "Hybrid resonant organic-inorganic nanostructures for optoelectronic applications," Chemical Review 111, 5179-5214 (2011).

[93] Q. Gu, M. Yuan, S. Ma, and G. Sun, "Structures and photoluminescence properties of organic-inorganic hybrid materials based on layered rare earth hydroxides," Journal of Luminescence 192, 1211-1219 (2017).

[94] K. Yan, J. Qin, Z. Liu, B. Dong, J. Chi, W. Gao, J. Lin, Y. Chai, and C. Liu, "Organic-inorganic hybrids-directed ternary NiFeMoS anemone like nanorods with scaly surface supported on nickel foam for efficient overall water splitting," Chemical Engineering Journal 334, 922-931 (2018).

[95] L. Mazzocchetti, E. Cortecchia, and M. Scandola, "Organic-Inorganic hybrids as transparent coatings for UV and X-ray shielding," ACS Applied Materials and Interfaces 1, 726-734 (2009).

[96] X. Chu, M. Guan, L. Li, Y. Zhang, F. Zhang, Y. Li, Z. Zhu, B. Wang, and Y. Zeng, "Improved efficiency of Organic/Inorganic hybrid near-infrared light upconverter by device optimization," ACS Applied Materials and Interfaces 4, 4976-4980 (2012).

[97] J. Weickert, F. Auras, T. Bein, and L. Schmidt-Mende, "Characterization of interfacial modifiers for hybrid solar cells," Journal of Physical Chemistry C 115, 15081-15088 (2011).

[98] M. Krumm, F. Pawlitzek, J. Weickert, L. Schmidt-Mende, and S. Polarz, "Temperature stable and optically transparent thin film Zinc Oxide aerogel electrodes As model systems for 3D interpenetrating Organic-Inorganic heterojunction solar cells," ACS Applied Materials & Interfaces 4, 6522-6529 (2012).

[99] K. Chang, Y. Chen, K. Chang, M. Shellaiah, and K. Sun, "Junction model and transport mechanism in *hybrid* PEDOT:PSS/n-GaAs *solar cells*," Organic Electronics 51, 435-441 (2017).

[100] J. Na, M. Kitamura, M. Arita, and Y. Arakawa, "Hybrid p-n junction light emitting diodes based on sputtered ZnO and organic semiconductors," Applied Physics Letters 95, 253303 (2009).

[101] M. Bernius, M. Inbasekaran, J. O'Brien, and W. Wu, "Progress with Light Emitting Polymers," Journal of the American Chemical Society 12, 1737, (2000).

[102] J. Mei, Y. Diao, A. Appleton, L. Fang, and Z. Bao, "Integrated materials design of organic semiconductors for field effect transistors," Journal of America Chemical Society 135, 6724-6746 (2013).

[103] S. Gelinas, A. Rao, A. Kumar, S. Smith, A. Chin, J. Clark, T. van der Poll, G. Bazan, and R. Friend, "Ultrafast long-range charge separation in organic semiconductor photovoltaic diodes," Science 343, 512-516 (2014).

[104] A. Mishra and P. Bauerle, "Small molecule organic semiconductors on the move: Promises for future solar energy technology," Angewandte Chemie 51, 2020-2067 (2012).

[105] V. Coropceanu, J. Cornil, D. Filho, Y. Olivier, R. Silbey, and J. Bredas, "Charge transport in organic semiconductors," Chemical Reviews 107, 926-952 (2007).

[106] J. Kwon, K. Son, J. Jung, T. Kim, M. Ryu, K. Park, B. Yoo, J. Kim, Y. Lee, K. Park, S. Lee, and J. Kim, "Bottom gate gallium indium zinc oxide thin film transistor array for high-resolution AMOLED display," IEEE Electron Device Letters 29, 1309-1311 (2008).

[107] H. Kim, S. Nam, J. Jeong, S. Lee, J. Seo, H. Han, and Y. Kim, "Organic solar cells based on conjugated polymers: history and recent advances," Korean Journal of Chemical Engineering 31, 1095-1104 (2014).

[108] S. Yoon, S. Lou, S. Loser, J. Smith, L. Chen, A. Facchetti, and T. Marks, "Fluorinated copper phthalocyanine nanowires for enhancing interfacial electron transport in organic solar cells," Nano Letters 12, 6315-6321 (2012).

[109] S. Woo, W. H. Kim, H. Kim, Y. Yi, H. Lyu, and Y. Kim, "8.9% single stack inverted polymer solar cells with electron rich polymer nanolayer modified inorganic electron collecting buffer layers," Advanced Energy Materials 4, 1301692 (2014).

[110] D. Chaudhary, A. Ghosh, R. Thangavel, and L. Kumar, "Bulk heterojunction hybrid solar cells with non-toxic, earth abundant stannite phase $CuZn_2AlS_4$ nanocrystals," Thin Solid Films 649, 202-209 (2018).

[111] S. Ratnasingam and S. Collins, "Study of the photodetector characteristics of a camera for color constancy in natural scenes," Journal of the Optical Society of America A 27, 286-294 (2010).

[112] S. Gunapala, S. Bandara, A. Singh, J. Liu, S. Rafol, E. Luong, J. Mumolo, N. Tran, D. Ting, J. Vincent, C. Shott, J. Long, and P. LeVan, "640×486 long-wavelength two color GaAs/AlGaAs quantum well infrared photodetector (QWIP) focal plane array camera," IEEE Transactions on Electron Devices 47, 963-971 (2000).

[113] D. Baierl, B. Fabel, P. Gabos, L. Pancheri, P. Lugli, and G. Scarpa, "Solution-processable inverted organic photodetectors using oxygen plasma treatment," Organic Electron 11, 1199-1206 (2010).

[114] E. Saracco, B. Bouthinon, J. Verilhac, C. Celle, N. Chevalier, D. Mariolle, O. Dhez, and J. Simonato, "Work function tuning for high-performance solution-processed organic photodetectors with inverted structure," Advanced Materials 25, 6534-6538 (2013).

[115] A. Kojima, K. Teshima, Y. Shirai, and T. Miyasaka, "Organometal halide Perovskites as visible light sensitizers for photovoltaic cells," Journal of the American Chemical Society 131, 6050-6051 (2009).

[116] L. Qiu, L. Ono, and Y. Qi, "Advances and challenges to the commercialization of organic-inorganic halide perovskite solar cell technology," Materials Today Energy 7, 169-189 (2018).

[117] M. Lee, J. Teuscher, T. Miyasaka, T. Murakami, and H. Snaith, "Efficient hybrid solar cells based on meso-superstructured organometal halide Perovskites," Science 338, 643-647 (2012).

[118] J. Noh, S. Im, J. Heo, T. Mandal, and S. Seok, "Chemical management for colorful, efficient, and stable Inorganic-Organic hybrid nanostructured solar cells," Nano Letters 13, 1764-1769 (2013).

[119] Y. Shirahata, K. Tanaike, T. Akiyama, K. Fujimoto, A. Suzuki, J. Balachandran, and T. Oku, "Fabrication and photovoltaic properties of ZnO nanorods/perovskite solar cells," AIP Conference Proceedings 1709, 020018 (2016).

[120] J. Bortoleto, M. Chaves, A. Rosa, E. Silva, S. Durrant, L. Trino, and P. Filho, "Growth evolution of self-textured ZnO films deposited by magnetron sputtering at low temperatures," Applied Surface Science 334, 210-215 (2015).

[121] M. Sessolo and H. Bolink, "Hybrid organic-inorganic light emitting diodes," Advanced Materials 23, 1829-1845 (2011).

[122] K. Morii, M. Ishida, T. Takashima, T. Shimoda, Q. Wang, M. Nazeeruddin, and M. Gratzel, "Encapsulation-free hybrid organic-inorganic light emitting diodes," Applied Physics Letters 89, 183510 (2006).

[123] J. Ryan, E. Palomares, and E. Ferrero, "Towards low-temperature preparation of air-stable hybrid light-emitting diodes," Journal of Materials Chemistry 21, 4774 (2011).

[124] M. Takada, T. Kobayashi, T. Nagase, and H. Naito, "Inverted organic light emitting diodes using different transparent conductive oxide films as a cathode," Japanese Journal of Applied Physics 55, 3-6 (2016).

[125] B. Lee, E. Jung, Y. Nam, M. Jung, J. Park, S. Lee, H. Choi, S. Ko, N. Shin,Y. Kim, S. Kim, J. Kim, H. Shin, S. Cho, and M. Song, "Amine based polar solvent treatment for highly efficient inverted polymer solar cells," Advanced 26, 494-500 (2014).

[126] A. Nirmal, A. Kyaw, W. Jianxiong, K. Dev, X. Sun, and H. Demir, "Light trapping in inverted organic photovoltaics with nanoimprinted ZnO photonic crystals," IEEE Journal of Photovoltaics 7, 545-549 (2017).

[127] J. Young, J. Kim, J. Roh, H. Kim, and C. Lee, "Efficiency improvement of organic photovoltaics adopting Li- and Cd-doped ZnO electron extraction layers," IEEE Journal of Photovoltaics 6, 930-933 (2016).

[128] J. Jeong, S. Nam, H. Kim, and Y. Kim, "Inverted organic photodetectors with ZnO electron collecting buffer layers and polymer bulk heterojunction active layers," IEEE Journal of selected Topics in Quantum Electronics 20, 1480-1482 (2014).

[129] H. Kim, M. Ryu, J. Youn, A. Yusoff, and J. Jang, "Photomask effect in organic solar cells with ZnO cathode buffer layer," IEEE Electronic Device Letters 33, 1480-1482 (2012).

[130] M. Takada, S. Furuta, T. Kobayashi, T. Nagase, T. Shinagawa, M. Izaki, and H. Naito, "Inverted organic light-emitting diodes with an electrochemically deposited zinc oxide electron injection layer," Journal of Applied Physics 120, 185501 (2016).

[131] P. Biswas, S. Baek, S. Lee, J. Kim, J. Park, S. Lee, T. Lee, and J. Myoung, "Oxygen vacancy induced red light emission from flexible inorganic micropatterned p-CuO/n-ZnO heterojunction light emitting diode," Applied Physics Letters 109, 171102 (2016).

[132] T. Thao, D. Long, V. Truong, and N. Dinh, "Preparation and characterization of nanorod-like TiO_2 and ZnO films used for charge transport buffer layers in P3HT based organic solar cells," AIP Conference Proceedings 1763, 030002 (2016).

[133] X. Guo, L. Tang, J. Xiang, R. Ji, K. Zhang, S. Lai, J. Zhao, J. Kong, and S. Lau, "Solution processable organic/inorganic hybrid ultraviolet photovoltaic detector," AIP Advances 6, 055318 (2016).

[134] A. Abliz, J. Wang, L. Xu, D. Wan, L. Liao, C. Ye, C. Liu, C. Jiang, H. Chen, and T. Guo, "Boost up the electrical performance of InGaZnO thin film transistors by inserting an ultrathin InGaZnO:H layer," Applied Physics Letters 108, 213501 (2016).

[135] N. Azhar, A. Shafura, I. Affendi, S. Shariffudin, I. Saurdi, S. Alrokayan, H. Khan, and M. Rusop, "Investigation of electrical and optical properties of MEH-PPV: ZnO nanocomposite films for OLED applications," AIP Conference Proceedings 1733, 020044 (2016).

[136] Y. Wu, C. Liao, P. Lee, Y. Liu, C. Liu, and C. Liu, "Organic/inorganic F8T2/GaN light emitting heterojunction," Organic Electronics 49, 64-68 (2017).

[137] M. Forsberg, E. Serban, E. Alexandra, C. Hsiao, M. Junaid, J. Birch, and G. Pozina, "Near band gap luminescence in hybrid organic-inorganic structures based on sputtered GaN nanorods," Scientific Reports 7, 1-7 (2017).

[138] P. Kumar, S. Guha, F. Shahedipour-Sandvik, and K. Narayan, "Hybrid n-GaN and polymer interfaces: Model systems for tunable photodiodes," Organic Electronics 14, 2818-2825 (2013).

[139] M. Shin, D. Gwona, C. Lee, G. Lee, I. Jeon, H. Ahn, S. Yi, and D. Ha, "Hybrid device based on GaN nanoneedles and MEH-PPV/PEDOT:PSS polymer," Materials Research Bulletin 68, 326-330 (2015).